APPENDIX G

Characterization of Slurry Phase Flow in the LaPorte AFDU using DP Measurements

ADDENDUM TO DOE REPORT

Characterization of Slurry-Phase Flow in the LaPorte Alternative Fuels Development Unit (AFDU) using Differential Pressure Measurements*

Kim A. Shollenberger and Timothy J. O'Hern
Sandia National Laboratories, Albuquerque, NM

EXECUTIVE SUMMARY

A methanol production run was performed at the LaPorte Alternative Fuels Development Unit (AFDU), a pilot scale slurry-phase bubble-column reactor in LaPorte, Texas, owned by the DOE and operated by Air Products and Chemicals, Inc. Slurry-phase bubble-column reactors are used extensively by chemical manufacturers to perform a wide variety of gas/liquid/solid reactions such as oxidation, hydrogenation, chlorination, aerobic fermentation and coal liquefaction (Shah and Deckwer, 1983). Differential pressure taps were added to the AFDU by Air Products prior to the run to allow measurement of average gas holdups along the column. The differential pressure technique was being tested for suitability in making gas holdup measurements for three-phase mixtures in columns too large to accommodate the gamma densitometer diagnostic currently used on the AFDU. Sandia contributed to this effort by providing a portable high-speed data acquisition system to monitor real-time pressures on site and by performing data analysis on the differential pressure data to determine gas holdup values. Validation of the technique was successfully completed and mean gas holdups up to 47% were measured. In addition, statistical analysis of the fluctuations in the pressure data confirmed that the column is generally operating in the churn-turbulent regime with up to 2% fluctuations in the gas holdup. Finally, differential pressures were measured during three Dynamic Gas Disengagement, or quick shutdown, experiments to estimate mean bubble diameters.

INTRODUCTION

The LaPorte AFDU, shown schematically in Figure 1, is a slurry-phase bubble column reactor. It is a tall cylindrical vessel, 18 in. (0.457 m) in diameter and 50 ft. (15.24 m) high, that contains a bundle of tubes which serves as an internal heat exchanger. During methanol production the column is filled with a slurry-phase mixture of an organic liquid and solid metallic oxide catalyst into which a gas mixture is injected at the bottom of the column. The gases adsorb into the liquid and react at catalytic sites on the solids to produce methanol and other hydrocarbon products which are continuously removed as a mixture of gases from the top of the vessel. Both temperature and pressure are controlled to optimize product distribution. The driving force for liquid recirculation is the gas rising through the liquid. A slurry-phase bubble column is used for this process because the organic liquid serves as an excellent heat sink for the highly exothermic reaction. The LaPorte AFDU can also be used for the Fischer-Tropsch reaction, where the liquid medium is molten wax and the product is additional liquid wax, which is continuously removed.

Drakeol 10, a light-weight mineral oil, was used as the organic liquid for the methanol production run reported here. At 482 °F (250 °C) its dynamic viscosity is 0.863 cSt and its density is

*Sandia is a multiprogram laboratory operated by Sandia Corporation, a Lockheed Martin Company, for the United States Department of Energy under Contract DE-ACO4-94AL85000.

701.7 kg/m^3 . Two commercially available catalysts (which we label catalyst A and catalyst B) and two gas mixtures (Texaco and Kingsport) were tested. Both catalysts are a combination of copper oxide, zinc oxide, and alumina with densities of 5.73 g/cm^3 and 4.88 g/cm^3 and reduction factors in weight (ϕ) after oxidation of 0.750 and 0.794 for catalyst A and B, respectively. Catalyst loadings $\omega_S = (m_S/\phi) / (m_S + m_L)$ for catalyst A ranged from 43.0% to 49.4% giving a volume fraction of solids in the slurry of 5.5% to 6.7%. Loadings for catalyst B ranged from 38.9% to 44.9% giving a volume fraction of solids in the slurry of 6.0% to 7.4%. The main components for the two gas mixtures used are as follows: Texaco is 34.7% H_2, 50.6% CO, 1.0% N_2 and 12.9% CO_2 giving a molar mass of 20.81 kg/kg-mol, and Kingsport is 60.9% H_2, 24.5% CO, 3.9% N_2 and 10.0% CO_2 giving a molar mass of 13.59 kg/kg-mol.

The superficial gas velocity, pressure, and temperature for the LaPorte AFDU are all generally kept very high, and it is assumed that good mixing with a uniform distribution of solids in the liquid is present. However, high gas velocities also dictate that the flow is in the churn-turbulent or strongly coalescing regime. Eventually, this flow regime will result in large inhomogeneities in the flow both spatially and temporally. If the individual gas pockets or fluctuations become large enough to push the reactor into a hydrodynamics-limited operation where the reaction rates are limited by mass transport to the catalyst, the efficiency of the process could suffer greatly. Therefore, it is important to monitor average gas holdups, their fluctuations, and bubble size distributions. Many previous researchers have measured these quantities, and some have done so in organic fluids and slurries (e.g. Krishna and Ellenberger, 1996; Wilkinson et al., 1992; Patel et al., 1989, Bukur et al.,1987; and O'Dowd et al.,1987), but always in much smaller diameter columns and never under the same operating conditions found in the AFDU. Because of the inability to extend correlations, particularly those for multiphase flows, outside the region for which they were derived, gas holdup must be monitored continuously while the AFDU is operating.

A standard, non-intrusive technique used for measuring gas holdup is gamma densitometry (GD). This technique is calibrated to relate the measured attenuation of a beam of gamma photons through a two or three-phase flow to its gas volume fraction or gas holdup. GD is currently used on the AFDU; however, because of the thick walls on the AFDU (1 in. or 2.54 cm steel) and the presence of an internal heat exchanger, it is only possible to obtain accurate measurements along the diameter of the column. If the gas holdup varies radially, GD cannot measure the volume averaged gas holdup without some knowledge of the gas holdup profile. Again, because of the highly attenuating walls, it is impossible to resolve temporal variations in gas holdup using GD. An alternative technique that can be used to determine gas holdup and its temporal fluctuations is the differential pressure technique where gas holdup is related to the static pressure head of a two or three-phase mixture located between the two pressure taps. Many previous researchers have used DP measurements to calculate average and instantaneous gas holdup, but not under the operating conditions found in the AFDU. Thus, the first objective for this project was to validate the use of the DP technique to measure average gas holdups under industrial conditions. The second objective was to determine the extent to which the instantaneous gas holdup values deviate from their mean and the frequency of these deviations. Finally, bubble size distributions and Sauter mean bubble diameters were estimated for three sets of operating conditions by measuring differential pressures during a Dynamic Gas Disengagement experiment, or quick shutdown test.

GAS HOLDUP CALCULATIONS

Gas holdup (ε_G) is a measure of the ratio of gas volume (V_G) to the total three-phase mixture volume (V). Thus, it quantifies how much gas is "held" up in the three-phase mixture. It can be related to the densities of the various components in the flow using a mass balance as follows:

$$m = m_S + m_L + m_G \tag{1}$$

where m is the total mass and the subscripts S, L and G correspond to solid, liquid and gas, respectively. Dividing through by total volume V yields:

$$\frac{m}{V} = \frac{m_S}{V_S}\frac{V_S}{V} + \frac{m_L}{V_L}\frac{V_L}{V} + \frac{m_G}{V_G}\frac{V_G}{V} \tag{2}$$

Substituting in the solid, liquid, gas and total density (or three phase density, ρ) and the gas and solids holdup (ε_S) and solving for ε_G:

$$\varepsilon_G = \frac{(\rho_L - \rho) + \varepsilon_S(\rho_S - \rho_L)}{(\rho_L - \rho_G)} \tag{3}$$

Differential pressure measurements are then used to calculate ρ within a bubble column using the fully developed momentum equation for upward turbulent flow in a tube:

$$\frac{dP}{dz} = \frac{\rho}{r}\frac{d}{dr}\left[(\nu_m + \nu_t) r \frac{dU}{dr}\right]_{r=R} + \rho g \tag{4}$$

where U is the local mean velocity of the slurry near the walls, and ν_m and ν_t are the momentum and turbulent diffusivity of the liquid, respectively. We can greatly simplify (4) by assuming that for a bubble column, where the net liquid flow is negligible, the shear stress term is small compared to the gravity force, giving the simple hydrostatic equation:

$$\rho = \frac{\Delta P}{g\,\Delta z} \tag{5}$$

This assumption has been validated for laboratory-scale slurry-phase bubble-column experiments at low gas flow rates by Daly (1990). However, in larger columns, as the liquid flow recirculation increases in velocity and turbulence intensity, this assumption needs to be verified for its continuing validity at all scales.

The final quantity needed to calculate gas holdup in (3) is the slurry density. For the AFDU, the total weight of catalyst initially added to the reactor is known, but the weight of liquid in the system varies as it is sometimes withdrawn and recirculated. Thus, one more independent measurement of the three-phase flow is needed to calculate the slurry density. For this experiment, a gamma densitometer is used to determine the total expanded height of the three-phase slurry mixture. The initial catalyst weight is then divided by the total volume to find the solids holdup:

$$\varepsilon_S = \frac{m_S/\rho_S}{V} \tag{6}$$

It should be noted that because a total volume method was used to close the three-phase equations, one of the phases must be assumed to be uniform throughout the column. In the following results, the solids are assumed to be uniformly dispersed throughout the liquid, which is in general a good assumption for a well mixed, high velocity flow in a large diameter column (Daly, 1990). Thus, (3), (5) and (6) can be used to calculate volume-averaged gas holdups between two locations using the corresponding differential pressure measurement and total expanded three-phase height.

DYNAMIC GAS DISENGAGEMENT TECHNIQUE

The gas holdup, together with the bubble size distribution, can be used to calculate interfacial area (A_S) using the following relations for spherical bubbles:

$$A_S = \frac{6\,\varepsilon_G\,V}{D_{32}} \tag{7}$$

$$D_{32} = \frac{\sum n_i\,D_i^{\,3}}{\sum n_i\,D_i^{\,2}} \tag{8}$$

where D_{32} is the Sauter mean diameter and n_i is the fraction of bubbles with diameter D_i. If the bubbles are too large to be spherical, an equivalent diameter is often used to relate surface area to volume. An estimate of the bubble size distribution can be obtained using the Dynamic Gas Disengagement (DGD) technique developed by Sriram and Mann (1977). A typical DGD experiment is performed in a transparent column and consists of quickly shutting down the gas being delivered to the column and measuring the rate at which the height or interface of the gas/liquid or gas/liquid/solid mixture falls with time. The velocity of the falling interface is then used to determine the velocity of the gas leaving the system. Differential pressures, however, measure the rate at which the gas holdup evolves with time between two pressure taps. Other researchers such as Daly et al. (1992), who have performed DGD experiments using differential pressure data, have simply used the data to estimate the rate at which the interface falls, assuming that the gas holdup measured between the taps equals the total volume-averaged gas holdup, and then followed the original derivation for determining bubble velocities. This is not necessary since the technique can easily be rederived to relate the velocity of the gas or bubble velocity (U_B) to the evolution of gas holdup in the volume between the pressure taps:

$$U_{B,i} = -\frac{\Delta z}{\varepsilon_{G,0}}\,\frac{d\varepsilon_{G,i}}{dt} \tag{9}$$

where Δz is the distance between the differential pressure taps, the subscript i indicates a bubble diameter range, and the subscript 0 represents an initial value. For this derivation, it is assumed that one bubble size class is disengaging between the pressure taps for each velocity calculated. This approximation is best for the taps located closest to the top interface and improves as the taps are

moved closer together. Of course, it must also be assumed for either method of analysis that the bubbles do not coalesce or break up during the disengagement process.

The number of bubbles in each bubble size class can be derived from conservation of mass:

$$N_{B,i} = \frac{\Delta\varepsilon_{G,i}\Delta z\, A}{\frac{\pi}{6} D_{B,i}^3} \tag{10}$$

Finally, the velocities are used to estimate the bubble diameter distribution using either Stokes' Law for small bubbles,

$$D_B = \left[\frac{18\mu_{SL}U_B}{g(\rho_{SL}-\rho_G)}\right]^{1/2}, \quad Re < 2 \tag{11}$$

a correlation by Peebles and Garber (1953) for midsize bubbles,

$$D_B = 4.67\left(\frac{\mu_{SL}}{\rho_{SL}}\right)^{0.41}\frac{U_B^{0.78}}{g^{0.59}}, \quad 2 \le Re \le 4.02\left(\frac{g\,\mu_L^4}{\rho_L\,\sigma^3}\right)^{-0.214} \tag{12}$$

or a correlation by Clift et al. (1978) for larger sized bubbles

$$U_B = \left[\frac{2.14\sigma_{SL}}{\rho_{SL}\,d_B} + 0.505g\,D_B\right]^{1/2}, \quad D_B > 1.3 \text{ mm} \tag{13}$$

Alternatively, a more recent correlation by Jamialahmadi, et al. (1994) can be used that has been tested for a wider range of fluid properties and is valid for all liquid Reynolds numbers.

$$U_B = \frac{U_{sp}U_w}{\sqrt{U_{sp}^2 + U_w^2}} \tag{14}$$

$$U_{sp} = \frac{1}{18}\left(\frac{\rho_{SL}-\rho_G}{\mu_{SL}}\right)g\,D_B^2\left(\frac{3\mu_{SL}+3\mu_G}{2\mu_{SL}+3\mu_G}\right) \tag{15}$$

$$U_w = \sqrt{\frac{2\sigma}{D_B\,(\rho_{SL}+\rho_G)} + \frac{g\,D_B}{2}} \tag{16}$$

All of these relations were developed for single bubbles rising through a quiescent liquid and it must be assumed that during the disengagement process neither liquid recirculation nor bubble interactions (i.e. swarming, wall effects, etc.) invalidate their use. The validity of this assumption improves for smaller gas holdups. In addition, these relations were developed for a continuous, pure liquid phase; clearly, the slurry properties, such as viscosity (μ_{SL}) and surface tension (σ_{SL}),

must be measured carefully. Finally, it is also assumed that negligible solid settling occurs during the disengagement process.

STATISTICAL ANALYSIS

The Introduction outlined the importance of determining the flow regime within the bubble column. Figure 2 shows differential pressure data that were recorded during a stable period of operation. Note that there are significant temporal fluctuations in the signal. Statistical techniques for analyzing the fluctuations in the pressure signal can be used to determine when the transition from a laminar, homogeneous bubbly flow to an inhomogeneous, churn-turbulent flow occurs. A review of previous efforts to use these techniques for quantifying various transitions in multiphase flows is given by Daly (1990).

One way to analyze the time varying component of the pressure signal involves calculating the magnitude of the fluctuations or standard deviation in the differential pressures. For bubbly flow where a single log normal distribution of gas bubbles exists, it is expected that the fluctuations should be negligible because of the uniformly distributed gas holdup. In churn-turbulent flow, if large slugs of gas are separated in the flow, the pressure will measure increasing fluctuations as the large waves of gas holdup rise in the column. A second technique is to use a Fourier transform to analyze the characteristic frequencies of the pressure readings. For bubbly flow, there should be no strong characteristic frequencies, but for churn-turbulent flow, the frequency should be a measure of the rate at which gas pockets move through the column.

UNCERTAINTY ANALYSIS

An uncertainty analysis provides information to determine the range of conditions under which it is feasible to use differential pressure measurements to calculate gas holdup. Moffat (1988) shows that when several independent variables are used to calculate a function $R(X_1, X_2,..., X_i)$, the individual terms contribute to the uncertainty δR by a root-sum-square as follows

$$\delta R = \left[\sum_{i=1}^{N} \left(\frac{\partial R}{\partial X_i} \ \delta X_i \right)^2 \right]^{1/2} \tag{17}$$

Applying this to the gas holdup, and assuming that the uncertainties in the single phase densities are negligible compared to the uncertainty in the measured three-phase density (i.e., $\delta\rho_G, \delta\rho_L, \delta\rho_S \ll \delta\rho$) leads to

$$\delta\varepsilon_G = \left[\left(\frac{\partial \varepsilon_G}{\partial \rho} \ \delta\rho \right)^2 + \left(\frac{\partial \varepsilon_G}{\partial \varepsilon_S} \ \delta\varepsilon_S \right)^2 \right]^{1/2} \tag{18}$$

and then substitute in (3) to obtain:

$$\delta\varepsilon_G = \left\{ \left[\frac{1}{(\rho_L - \rho_G)} \delta\rho \right]^2 + \left[\frac{(\rho_S - \rho_L)}{(\rho_L - \rho_G)} \ \delta\varepsilon_S \right]^2 \right\}^{1/2} \tag{19}$$

Performing the same analysis on (5) and (6) gives:

$$\frac{\delta\rho}{\rho} = \left[\left(\frac{\delta\Delta P}{\Delta P}\right)^2 + \left(\frac{\delta\Delta z}{\Delta z}\right)^2\right]^{1/2} \tag{20}$$

$$\frac{\delta\varepsilon_S}{\varepsilon_S} = \left[\left(\frac{\delta m_S}{m_S}\right)^2 + \left(\frac{\delta V}{V}\right)^2\right]^{1/2} \tag{21}$$

Finally, combine (19), (20), and (21) and rearrange to get

$$\delta\varepsilon_G = \left[\frac{(\rho_S - \rho_L)}{(\rho_L - \rho_G)}\ \varepsilon_S\right]\left\{\left[\frac{\Delta P/(g\ \Delta z)}{\varepsilon_S\ (\rho_S - \rho_L)}\right]^2 (u_{\Delta P}{}^2 + u_{\Delta z}{}^2) + u_{m_s}{}^2 + u_V{}^2\right\}^{1/2} \tag{22}$$

where u denotes relative uncertainty in the subscripted variable. If we substitute in values for the above variables that represent typical operating conditions in the AFDU ($\Delta z = 3$ m $\pm$ 0.03 m, $m_S = 400$ kg $\pm$ 4 kg, $V = 70$ ft.^{3} $\pm$ 0.7 ft.^{3}), use property values for Texaco gas and catalyst A (listed in the Introduction Section), and use the uncertainty specified for the pressure transducers (given in the Experimental Equipment Section), we can calculate the relative uncertainty in the gas holdup ($u_{\varepsilon_G} = \delta\varepsilon_G/\varepsilon_G$) as a function of gas holdup as shown in Figure 3 (a). For gas holdups greater than 35% the relative uncertainty is less than 0.029 corresponding to $\delta\varepsilon_G = 1.03\%$. Figure 3 (b) shows the relative uncertainty in the gas holdup as a function of the distance between the pressure taps (Δz) obtained by again starting with (22), substituting in the above values, and by using $\varepsilon_G = 35\%$. This figure shows that Δz can decrease to 0.5 m before any significant increases in uncertainty are experienced. Thus, gas holdup can theoretically be measured with good accuracy using the differential pressure technique under industrial conditions if the assumptions made to reduce the full momentum equation to the hydrostatic equation are correct.

EXPERIMENTAL EQUIPMENT

Rosemount Alphaline pressure transducers (model 1151) were selected and installed on the AFDU by Air Products and Chemicals. They are industrial-quality transducers that measure differential pressures directly using a diaphragm and a δ-cell capacitance sensing element. The maximum span of the selected transducers is 0-10.8 psid (74.4 kPa) with an accuracy of $\pm$0.003 psid (20.7 Pa). The stability of the readings is guaranteed to 0.005 psid (34.5 Pa) with a zero error of less than 0.0135 psid (93.1 Pa) for up to six months of operation. Remote seal systems, from the same manufacturer, were used to measure the differential pressure directly between nozzles C to N2, N2 to D and D to N1 as shown in Figure 1. Differential pressures at nozzles N1 and E were both taken with reference to the gas pressure above the liquid slurry. The transducers themselves have adjustable damping with a minimum damping of 0.2 seconds. The remote seals, which use oil filled transmission lines, also add some damping to the measurement. The extent of this damping can be determined experimentally as shown in the next section, Temporal Analysis of Differential Pressures.

Readings from the transducers were recorded using an existing Bailey operations control and monitoring unit. However, this system is currently configured to collect data at a rate of 1 sample

every 5 seconds. It was desired to sample data at higher frequencies for the DGD tests and for the statistical analysis. Sandia provided a portable data acquisition unit to accomplish this. The system consisted of a National Instruments SCXI (Signal Conditioning and Instrumentation System) that was connected via a parallel port to a notebook computer. Data acquisition was automated using a LabView program. The SCXI is capable of acquiring data using an enhanced parallel port at rates up to 100 kHz. An isolation amplifier was required for use as one of the plug-in modules in the SCXI to protect the equipment from surges and ground loops that result from having two independent data acquisition systems recording the same signal. Finally, an external mass data storage unit (150 MB Bernoulli Transportable) was needed to handle the large volume of data acquired during the entire run.

TEMPORAL ANALYSIS OF DIFFERENTIAL PRESSURES

Several pressure data files were acquired for analysis at different sampling rates. These files were first examined to determine what sampling frequency would be adequate. Although very fast data rates are possible, data management becomes more cumbersome, eventually without adding any information due to the frequency response limitations of the transducers. Shown in Figure 2 is a time trace of pressures measured at three different frequencies for the transducer located between nozzles N2 and D acquired during Run No. 13.1 (see Table 1). The difference between the 2.0 Hz data and the 1.0 Hz data is negligible, but there is significant filtering of the higher frequencies at 0.2 Hz. Thus, these data suggest for this flow rate that the higher sampling rate of 1.0 Hz is required to analyze the measured frequencies of the flow. Furthermore, the sampling rate of 1.0 Hz is shown to be sufficiently fast by comparison to the 2.0 Hz data. Pressures were also collected at a rate of 1000 Hz. This rate is significantly higher than the response time of the transducers, and variations in readings should be an indication of the amount of noise in the signal. Fluctuations of pressures were measured to be less than 0.003 psid (20.7 Pa) which agrees with the specifications for the transducers and is 0.3% of the magnitude of fluctuations being measured at the 1.0 Hz sampling rate. Thus, the pressure fluctuations being measured in the column are significantly greater than the signal noise and represent actual fluctuations in pressure.

EXPERIMENTAL RESULTS

The LaPorte AFDU was operated over a period of one month over a range of flow conditions that are outlined in Table 1. The following conditions were kept constant throughout the run: three phase mixture height at 43.5 ft. (13.26 m or L/D = 29) and temperature at 482 °F (250 °C). Pressure during each run was held constant, usually at 750 psia (5.17 MPa) or 765 psia (5.27 MPa), except for R13.3 whose pressure was 735 psia (5.07 MPa) and R14.3 whose pressure was 535 psia (3.69 MPa). Two commercially available catalysts were used (catalyst A for the R13 series and catalyst B for the R14 series). Both catalysts were added in one measured dose at the beginning of each run series and, because liquid was added or withdrawn to keep the total expanded three-phase height constant as gas holdup varied, the catalyst loading also varied. The loadings by mass (ω_S) ranged from 43% to 49% for catalyst A and from 39% to 45% for catalyst B. Finally, two gas mixtures (Texaco and Kingsport) and four inlet superficial gas velocities (U_G = 0.046, 0.15, 0.26 and 0.36 m/s) were tested.

Average Gas Holdups

Volume-averaged gas holdup values were obtained by averaging differential pressure measurements over long periods of time and along the column during a stable run. Each run was broken into two periods to check the stability of the catalyst and measurements. Tables 2 and 3 show the averaged data and calculated catalyst loadings along with values obtained using a gamma densitometer system and from a shutdown test. The gamma densitometer measures gas holdup by comparing the attenuation for the three phase-flow to that of the empty and full vessel using a ray through the diameter of the vessel and by using the three-phase expanded height measurement. The gamma densitometer measurements can be made at any elevation and were taken along the length of the vessel and averaged. Scans were recorded about every 5 hours during each stable operating period. A shutdown test consists of measuring the expanded three-phase mixture height (H), using the gamma densitometer, shutting off the gas supply, and then measuring the two-phase mixture height (H_S). The gas holdup is then calculated using $\varepsilon_G = (H - H_S) / H$. Because H and H_S can be measured with good accuracy, the shutdown test provides the most accurate measurement of gas holdup volume averaged over the entire vessel.

The gas holdups given in Tables 2 and 3 are shown graphically in Figure 4. As can be seen in the figures, the gamma densitometer measured gas holdups are systematically 7.0% to 14.3% higher than the values obtained using the differential pressure technique. For the three gas holdups obtained using the shutdown test, the agreement with the differential pressure measurements is very good (within 3.0%). Thus, it appears there is a systematic error in the densitometry readings which can be linked to the assumption that the flow is radially homogeneous (needed to calculate area averaged gas holdup using only one chord of data). However, a radial distribution of gas holdup is generally observed in two-phase and slurry-phase flows, such that gas holdup is highest at the centerline and decreases toward the edges (Bukur et al., 1987, Dudukovic et al., 1991). For such a profile, the data averaged along the diameter would give too much weight to the area with highest gas holdup at the centerline and therefore would overestimate the average gas holdup. This appears to be the case for the gamma densitometer measurements made on the AFDU. Since the radial gas holdup distribution in the AFDU cannot currently be directly measured or predicted, this result is useful in letting us infer that a customary gas holdup profile is present.

To consider the effect of changing the catalyst or volume fraction of solids, we can compare Figure 4a to Figure 4b. It is found that the 0.5% to 1.9% increase in solids volume fraction resulted in a 7.0% to 8.4% decrease in gas holdup at the same superficial velocity. It is difficult to conclude why this occurs from the limited data set. Two factors that probably contribute are (1) the increase in the volume of solids will simply displace the gas, and (2) the increased volume of solids will probably decrease surface tension and increase viscosity which enhances coalescence and decreases gas holdup.

In Figures 4a and 4b, the Texaco and Kingsport gases are represented by closed and open symbols, respectively. The best comparison of the effect of gas composition on gas holdup can be made by looking at run numbers R14.2 and R14.4 which are at approximately the same flow conditions (see Table 1). We find that the gas holdup is 4.7% lower for the Kingsport gas at $U_G = 0.15$ m/s. Furthermore, if we linearly extrapolate a gas holdup value for the Kingsport gas to compare to the measured Texaco gas values we calculate decreases in gas holdup of 5.7% for catalyst A and 6.7%

for catalyst B, both at U_G = 0.26 m/s. For the same superficial gas velocity (or volume flow rate) the mass flowrate for the Kingsport gas will be lower because its density is lower (16.3 kg/m^3 versus 25.0 kg/m^3 at typical AFDU conditions). If we compare gas holdups for the same mass flow rate ($U_{G,\,Texaco} = (\rho_{G,\,Kingsport}/\rho_{G,\,Texaco})U_{G,\,Kingsport}$ giving $U_{G,\,Texaco}$ = 0.26 m/s for $U_{G,\,Kingsport}$ = 0.36 m/s) the differences in gas holdup reduce to 1.75% for catalyst A and 2.83% for catalyst B. This suggests that both the volume and momentum flux of the gas leaving the sparger are important for correlating gas holdup.

Figure 4b also demonstrates trends in the gas holdup with superficial gas velocity. It is seen that the slope of the straight line fit between the three points decreases with superficial gas velocity. This corresponds again to the type of curve one would expect to see in any two or three-phase flow in a large-diameter column where slugs do not form. Generally, the curves have two regions. The first region has a constant steep slope corresponding to bubbly flow where bubbles move through the column without interaction and the slope can be derived from continuity. When the bubbles begin interacting (i.e. coalescing and swarming) the gas holdup increases less as the gas velocity continues to increase. This region corresponds to the churn-turbulent regime. From the graphs, it appears that the three highest flow rates may be in the churn-turbulent regime and that the lowest flow rate is either in a bubbly flow or transition regime. As stated in the Introduction, a statistical analysis will be used later as a more definitive means for determining which flow regimes is present.

Figures 5 through 11 show the variations in gas holdups averaged over one-hour periods for the duration of each run where L/D is the axial distance above the sparger, non-dimensionalized with respect to the diameter of the AFDU. Graphs for run numbers R13.2 and R14.9 are omitted because data were taken for only 3 hours in each case and the values are relatively constant over that period. In all of these plots, gas holdups tend to drift both up and down with time and occasionally experience fairly large disturbances. For example, Figure 6 shows a large increase in gas holdup at the uppermost location that coincides with a decrease of similar magnitude at the bottom three locations. These disturbances were observed for both gases and catalysts and appear in the column for each velocity tested. Looking at the hourly run schedule, it was found that the fluctuations correspond to periods when the GD system is taken from its normal operation of monitoring overall expanded three-phase mixture height to scan the axial variation in gas holdup. While this is done, liquid is no longer added to maintain a constant height. Apparently, the liquid level drops enough during this period, possibly below the uppermost tap, resulting in an increase in gas holdup between the top two pressure taps. Conversely, between the lower pressure taps, the decrease in liquid level decreases gas holdup. This can be explained by realizing that the solids loading will increase as the liquid level drops, but, for these calculations we must use the original solids loading obtained before the axial gamma scan. From (3), the underestimated solids holdup will also lead to calculated gas holdups that are artificially low for this time period.

Axial Variations in Average Gas Holdups

From the four differential pressure sections along the column (see Figure 1), the axial variation of the gas holdup along the column length can be measured. The data are presented in Tables 4 and 5

and plotted in Figures 12a and 12b. For each superficial gas velocity and for both catalysts and gases, the variations in gas holdup with axial location follow the same trends. This suggests that all of the trends noted above for the volume-averaged data remain valid at each elevation. In Figures 12a and 12b, it is also shown that the gas holdup initially decreases with elevation (by about 3%) and then increases (by 2.3%) and finally increases significantly (by 7%). This seems contrary to the anticipated drop in gas holdup expected as a result of the gases reacting to form a denser gas. Compositions of the inlet and exiting gases were monitored during each of the runs. For the Texaco gas, the densities were typically 25.0 kg/m^3 at the inlet and 30.2 kg/m^3 at the outlet corresponding to a decrease in gas holdup of about 7% for an initial gas holdup of 40%. For the Kingsport gas, the densities were typically 16.0 kg/m^3 at the inlet and 21.9 kg/m^3 at the outlet corresponding to a decrease in gas holdup of about 10% for an initial gas holdup of 40% (except for the highest velocity cases). The axial gas holdup distributions never reflect these changes in gas holdup which are expected from the gas contraction during reaction. A possible explanation for the shape of this profile (i.e. increasing gas holdup versus decreasing at higher L/D) is that there are two competing effects determining the axial gas holdup distribution. Initially, a high gas holdup is seen near the sparger where a dense "bubble cloud" forms. As the gas moves up the column, it forms distinct bubbles with a distribution of sizes that begin to react resulting in an initial drop in gas holdup. The bubbles continue to decrease in size further along the column until a significant decrease in their rise velocity causes the gas holdup to begin increasing. This continues and possibly results in a foaming region at the top of the vessel.

Statistical Analysis of Gas Holdups

The use of statistical analysis to discern flow regime transitions will be discussed here. The data are presented in Tables 6 and 7. Figures 13a and 13b show standard deviations in gas holdup (σ) versus superficial gas velocities (U_G) and axial distance for each catalyst. Note that in these figures closed and open symbols again denote the Texaco and Kingsport gases, respectively. For both catalysts, we see that σ increases with U_G as expected, possibly showing that gas pockets are increasing in size and/or number. For the lowest velocity case, σ is 0.25% which corresponds to a pressure standard deviation of 0.01 psid (68.9 Pa). This is higher than the 0.003 psid (20.7 Pa) range of the transducers and shows that even for the lowest velocity case there exists measurable fluctuations in the flow. Comparing Figures 13a and 13b we see that there is a measurable decrease in standard deviation as L/D increases for catalyst A that is not seen for catalyst B, whose gas holdup is about 7.7% lower. In Figure 13b, we also see that σ no longer depends on gas type, which also changes gas holdups by about 6.0%. Thus, the change in gas holdup caused by switching gases does not appear to be a critical parameter in determining the flow regime and other variables, such as volume of solids, may play a greater role. Finally, in Figures 13a and 13b we see that at the highest elevation in the column (L/D = 24.5) there is a significant increase in standard deviation. This may be the result of the liquid level falling below the top pressure nozzle for a significant period of time.

An example of a frequency spectrum obtained from a Fourier transform analysis of 3600 points of differential pressure data is shown in Figure 14 for a high velocity case (R14.3). This spectrum shows that there is a wide band of frequencies present but that there is a fairly broad peak in the spectrum centered at about 0.05 Hz. This suggests that a large pocket of gas either enters or leaves the region between the pressure nozzles every 20 seconds. An experimental effort is currently

being pursued at Sandia to verify which physical phenomena relate to the various frequency components being measured. Figures 15a and 15b show the strongest frequency components for each catalyst as a function of superficial gas velocity. The points represent values taken from each elevation and for each gas but are not noted separately on the graphs because there is no discernible dependency on either of these parameters. For both cases we see that the frequency increases with U_G and that there does not appear to be a dominant frequency for U_G less than 0.15 m/s. As stated earlier, the beginning of the appearance of a dominant frequency is an indication that gas pockets are present and that a transition to churn-turbulent flow has begun. Thus, the flow appears to be in the churn-turbulent regime for all but three of the run conditions tested. If we compare the graphs for the two catalysts, we see that the frequencies at 0.25 m/s are much lower for catalyst A, indicating that increasing the volume fraction of the catalyst results in an earlier transition to churn-turbulent flow.

Dynamic Gas Disengagement

Gas holdups were recorded after a quick shutdown of the gas entering the column for a Dynamic Gas Disengagement (DGD) analysis. The general technique for obtaining bubble size distributions using DGD has been outlined in an earlier section. Data were recorded for three sets of conditions, each following one of the long stable run periods (R13.2, R14.1 and R14.3). Table 1 shows that these cases represent three different flow rates, both gases and both catalysts. Shown in Figures 16 through 18 are DGD curves of gas holdup versus time for each of the runs, where the shutdown occurred at time zero. After shutdown, gas holdups between the bottom three nozzles (from L/D = 3.1 to 14.4) fall to approximately zero, indicating that all three nozzles are submerged in the pure slurry. The final gas holdup between L/D = 14.4 and 21.0 is between zero and unity, showing that the final slurry height is located between the two pressure taps. Finally, at the top location (L/D = 21.0 to 27.6) the gas holdup increases to unity, indicating that both upper nozzles are above the slurry level after shutdown.

One issue to address before interpreting the DGD data obtained from the differential pressures is that we are using the steady state momentum equation to calculate a dynamic effect. Assuming the Navier-Stokes equations are still valid for the catalyst suspension, the unsteady momentum equation includes an acceleration term that should be used, in addition to the viscous damping term (that we already neglected in the steady state analysis). These new terms require values for the liquid velocities and turbulent viscosity to be calculated. Because we do not know the magnitude of these variables, we can only assume that these terms are negligible with respect to the hydrostatic pressure. To numerically test this assumption would be difficult since a full model simulation is intractable. The best validation that could be achieved at this time was to measure DGD curves in a three-phase system (air/water/80 micron glass beads) in a 0.19 m column at atmospheric temperature and pressure using the differential pressure technique along with a high-speed video system. Figure 19 shows DGD curves for the three-phase system for two sets of differential pressures along the column, where the initial height of the liquid was L/D = 6, the solids loading is 40% by mass and the superficial gas velocity is 0.088 m/s. In this figure, the gas holdups from the two sets of differential pressure data should be averaged to compare them with the volume averaged video observations. We see that the measurements agree reasonably well. These graphs were obtained by averaging the differential pressure data over a 0.5-second interval because the signals contained many large-scale fluctuations. These fluctuations must be the result of the

ignored acceleration terms, but the numerical averaging of the differential pressures used to obtain these curves results in a disengagement curve that agrees with the high-speed video data. These results provide some validation for the use of averaged differential pressure data to obtain DGD disengagement curves.

Comparing Figures 16 through 18 to Figure 19, we see that none of the oscillations observed in the air/water/glass test case are present in the AFDU data. One explanation for the difference in the curves could be the difficulty in obtaining a quick enough shutdown of the gas supply to the AFDU. The inlet gas line is about 2 inches in diameter and is closed using a pneumatic flow control valve that will experience some lag. In future tests, monitoring the pressure downstream of the control valve would give a direct measurement of the rate at which the gas stops flowing and would make more accurate interpretation of the DGD curves possible. In addition, increased viscosity, measurement volume, and column height probably contributed to the smoothing of these curves. The other difference between these graphs is the shape of the disengagement curves. For a bubbly flow with a homogeneous distribution, one would expect the bubbles to disengage uniformly, leading to a single slope. For churn-turbulent flow, it was shown by Patel et al. (1989) that the two bubble classes usually lead to two distinct slopes: an initial steep slope for the large, high velocity gas pockets followed by the gradual slope of the slower moving small bubbles. These two slope regions are distinctly visible in Figure 19 but are not present in Figures 16 through 18. Again, this seems to indicate that the gas shutdown may have been too slow to measure both bubble classes, especially since the average and statistical gas holdup data give good evidence that the churn-turbulent regime exists at these flow rates.

Figures 20 through 24 compare the disengagement curves for all four elevations. At the lowest elevation, Figure 20, there is only a small change in slope between the lowest velocity case (R13.2) and the other two curves. At the next elevation, shown in Figure 21, there is a significant time lag between all three curves and again a similar change in slope. Thus, in the lowest portion of the column, there appears to be little difference in the disengagement process for the different flow conditions, but further up significant differences become present. We also see in Figures 20 and 21 that the disengagement curves do not quite go to zero, yielding final (post-shutdown) gas holdups of 2.32%, 2.40% and 0.75% at L/D = 3.1 to 7.9 and -1.63%, -1.34% and -1.46% at L/D = 7.9 to 14.4 for run numbers R13.2, R14.1 and R14.6, respectively. These offsets are slightly greater than the 1% gas holdup error that would be expected from drifts in the zeroing of the transducers alone. Therefore, these offsets represent a slight deviation from uniform solids loading. If the slurry density is lower at the top of the column, this would cause an overestimate in gas holdup, and correspondingly the higher slurry density at the bottom would result in an underestimate of gas holdup. In all of the cases, however, the deviations from zero are very small, confirming that the uniform solids loading assumption for the AFDU conditions is fairly good.

Next, Figure 22 shows the disengagement curves for pressure taps between L/D = 14.4 and 21.0. Here we see the that all three curves begin responding to the disengagement after about 10 seconds, and that they finish disengaging in the order of highest to lowest gas holdup. After complete disengagement, the final L/D location of the slurry level agrees with the average gas holdup measurements made during the stable run. Finally, Figure 23 shows the disengagement curves for pressure taps between L/D = 21.0 and 27.6. Again, the slopes are increasing and the duration of the disengagement is decreasing as the superficial gas velocity increases.

The gas holdups calculated between nozzles D and N2 are next converted to bubble velocities using (9). Bubble diameters can then be determined using either (11)-(13) or (14)-(16). Figure 24 shows the differences in the predicted terminal velocities between the correlations. It is seen that they agree reasonably well except for bubbles less than 0.2 cm in diameter. However, because we need to calculate bubble diameter from bubble velocity and since the graphs are non-monotonic, bubbles in the range of 0.1-0.3 cm for (11)-(13) and 0.05-0.25 cm for (14)-(16) cannot be measured using this kind of DGD analysis. This is a significant limitation of the technique and should be acknowledged when looking at the bubble diameter histograms presented later in this section.

The correlation by Jamialahmadi's et al. (1994) was tested for a wider range of fluid properties so it was used for the current DGD analysis. The properties of the slurry mixture used in (14)-(16) can be difficult to predict and will vary throughout the column, therefore Figures 25 through 27 are included to show the effects of surface tension, slurry viscosity and slurry density on the correlation by Jamialahmadi et al. (1994). For these figures and in the following analysis the slurry viscosity is estimated as a function of the volume fraction of solids in the liquid using a correlation by Thomas (1965). It ranges from 7.93×10^{-4} to 8.35×10^{-4} N•m/s^2. The surface tension used is 0.02 N•m which was given by the manufacturer of Drakeol 10 for pure liquid at 482 °F (250 °C). Gas density and gas viscosity had a negligible effect on the correlation. In all of the figures it is seen that the effect of variations in fluid properties is most pronounced for smaller bubble sizes and that there will be significant uncertainty in the analysis as fluid properties change. However, the graphs do become monotonic at low surface tension or for high viscosities which could, for certain operating conditions, help improve the accuracy of a DGD analysis.

Figures 28 through 30 show (a) the number of bubbles in each diameter class measured and (b) the corresponding volume distribution. Each of the number histograms (a) generally look like typical log-normal distributions with increasing bubble sizes as we go from R13.2 to R14.1 to R14.3. For the R14.3 histogram it appears that a second peak in the larger diameter range may be beginning to appear. The volume distributions in Figures 28 (b) to 30 (b) show one peak for R13.2 and roughly two peaks for R14.1 and R14.3.These results agree with the conclusions drawn in the Statistical Analysis section. For the low-velocity case, where the statistical analysis predicted a homogeneous bubbly flow, the DGD analysis produced a single small bubble size class. For the two higher velocity cases, where the statistical analysis predicted a heterogeneous, churn-turbulent flow, the DGD analysis suggests that two bubble size classes may have emerged with regards to volume fraction. In all three cases it is also shown in Figures 28 through 30 (b) that the bulk of the gas volume is carried by the largest bubbles which are vastly outnumbered by the smaller bubbles.

Finally, Sauter mean diameters can be calculated from the bubble size distributions. The results are as follows: D_{32} = 0.436 mm for R13.2, D_{32} =0.958 mm for R 14.1, and D_{32} =1.21 mm for R14.3. As the above histograms suggested, Sauter mean diameter appears to be increasing with gas velocity, but recall that both the gas and catalyst type also changed for these three runs and may be contributing to these changes. Interestingly, even though the superficial gas velocity and Sauter mean diameter are highest for R14.3, because of the change in gas composition, its average gas holdup is lower than that for R14.1. The only reasonable comparison for these values currently available was reported by Daly et al. (1992) who also used the DGD technique. They obtained Sauter mean diameters ranging from 0.5 to 2.0 mm for superficial gas velocities ranging from 0.02 to 0.1 m/s for nitrogen flowing through paraffin based reactor waxes in a 0.21 m column at 265 °C

and atmospheric pressure. The velocities for the LaPorte data were all higher (0.15-0.36 m/s), pressures were much higher (535-765 psia or 3.69-5.89 MPa), and the continuous phase was a slurry (catalyst loadings of 39% to 49% by weight). The diameters obtained in this study lie within the range measured by Daly et al. (1992).

CONCLUSIONS

The ability to use differential pressure measurements, combined with a knowledge of the solids loading, to accurately determine gas holdups in a slurry-phase bubble column reactor has been established as an industrially viable technique. Differential pressures were recorded for four different superficial gas flow rates, two gases and two catalysts at four axial locations. Increasing superficial gas velocity increased gas holdups as expected. Switching from Texaco to Kingsport gas, which contains a higher percentage of hydrogen and is less dense, decreased the total volume-averaged gas holdup by about 6%. Increasing the volume fraction of solids in the slurry by 0.5% to 1.9% decreased the total volume-averaged gas holdup by 7.0% to 8.4%. Variations in gas holdups along the vessel were similar for all conditions tested. In general, they decreased by about 3% and then actually increased overall by about 10% (where a total decrease in volume for the reacting gas would be expected). Using data obtained with the gamma densitometer, we were also able to hypothesize that the gas holdup profile is highest in the center of the vessel and decreases towards the walls.

Fluctuations in the differential pressure measurements were investigated using statistical analyses to determine when transitions in flow regime occur. Standard deviations and peaks in the frequency spectrum have been used to indicate that all but the lowest two velocity cases are in the churn-turbulent flow regime. The transition to the churn-turbulent flow regime did not seem to depend on the variations in gas holdup caused by switching gases but was accelerated by increasing the volume fraction of catalyst. Finally, a dynamic gas disengagement analysis was performed to determine bubble size distributions. This diameter was found to increase with superficial gas velocity. The shutdown tests were also used to infer that solids loading was axially uniform under the AFDU operating conditions.

ACKNOWLEDGMENTS

The authors wish to thank the Air Products and Chemicals personnel at the LaPorte AFDU for their cooperation and assistance, especially Bharat Bhatt, Ed Heydorn and Steve Cochrain. The authors also wish to acknowledge the efforts of John O'Hare and John Henfling of Sandia National Laboratories. The financial support of DOE PETC is gratefully acknowledged.

NOMENCLATURE

Variables

A	cross-sectional area of bubble column, m^2
A_S	gas/liquid interfacial area, m^2
D	column diameter, m
D_{32}	Sauter mean diameter, m
D_B	bubble diameter, m

g	gravitational acceleration, m/s^2
L	axial distance along column, m
m	mass, kg
n_A	molar fraction of component A
P	pressure, psi
r	radial location, m
R	radius of bubble column, m
Re	Reynolds Number
u_x	percent error in x
U	average liquid velocity, m/s
U_B	bubble velocity, m/s
U_G	superficial gas velocity, m/s
V	total (three-phase) volume, m^3
z	axial location, m
δR	uncertainty in value of R
Δz	distance between pressure taps, m
ε_n	holdup, ratio of volume of nth component to total volume
ϕ	catalyst weight reduction factor
μ	viscosity, N•m/s^2
ν_m	momentum diffusivity, m^2/s
ν_t	turbulent diffusivity, m^2/s
ρ	density, kg/m^3
σ	surface tension, N/m
ω_S	catalyst loading by weight, $(m_S / \phi) / (m_S + m_L)$

Subscripts

0	initial
G	gas
L	liquid
S	solid
SL	slurry

REFERENCES

Bukur, D. B., Patel, S. A., and Matheo, R., "Hydrodynamic Studies in Fischer-Tropsch Derived Waxes in a Bubble Column," *Chemical Engineering Communication*, **60**, 63, 1987.

Clift, R., Grace, J. R., and Weber, M. E., Bubbles Drops and Particles, Academic Press, 1978.

Daly, J. G., Hydrodynamic Studies in Two and Three-Phase Slurry Bubble Column Reactors, Ph. D. Dissertation, Texas A&M University, 1990.

Daly, J. G., Patel, S. A., and Bukur, D. B., "Measurement of Gas Holdups and Sauter Mean Diameters in Bubble Column Reactors by Dynamic Gas Disengagement Method," *Chemical Engineering Science*, **47**, 3647, 1992.

Dudukovic, M. P., Devanathan, N., and Holub, R., "Multiphase Reactors: Models and Experimental Verification," *Revue De L'Institut Francais Du Petrole*, **46**, 1991.

Jamialahmadi, M., Branch, C., and Müller-Steinhagen, H., "Terminal Bubble Rise Velocity in Liquids," *Chemical Engineering Research & Design*, **72**, 119, 1994.

Krishna, R., and Ellenberger, J., "Gas Holdup in Bubble Column Reactors Operating in the Churn-Turbulent Flow Regime," *AIChE Journal*, **42**, 2627, 1996.

Moffat, R. J., "Describing the Uncertainties in Experimental Results," *Experimental Thermal and Fluid Science*, **1**, 3, 1988.

O'Dowd, W., Smith, D. N., Reuther, J. A., and Saxena, S. E., "Gas and Solids Behavior in a Baffled and Unbaffled Slurry Bubble Column," *AIChE Journal*, **33**, 1959, 1987.

Patel, S. A., Daly, J. G., and Bukur, D. B., "Holdup and Interfacial Area Measurements Using Dynamic Gas Disengagement," *AIChE Journal*, **35**, 931, 1989.

Peebles, F. N., and Garber, H. J., "Studies on the Motion of Gas Bubbles in Liquids," *Chemical Engineering Progress*, **49**, 88, 1953.

Shah, Y. T., and Deckwer, W. D., "Hydrodynamics of Bubble Columns," Handbook of Fluids in Motion, ed. Cheremisinoff, N. P., and Gupta, R., Ann Arbor Science Publishers, Michigan, 1983.

Sriram, K., and Mann, R., "Dynamic Gas Disengagement: A New Technique for Assessing the Behavior of Bubble Columns," *Chemical Engineering Science*, **32**, 571, 1977.

Thomas, D. G., "Transport Characteristics of Suspension: VIII. A Note on the Viscosity of Newtonian Suspensions of Uniform Spherical Particles," *Journal of Colloid Science*, **20**, 267, 1965.

Wilkinson, P. M., Spek, A. P., and Van Dierendonck, L. L., "Design Parameters Estimation for Scale-up of High-Pressure Bubble Columns," *AIChE Journal*, **38**, 544, 1992.

Table 1. Table of conditions for a methanol/hydrodynamics run at the LaPorte Alternative Fuels Development Unit (AFDU) during June 1995.

Run No.	Hours Running	Gas Type	Reactor Pressure (psia)	Reactor Temp. (deg. F)	Superficial Gas Velocity (m/s)	Weight% of Catalyst Oxide
Catalyst A Runs						
R13.1	58.5	Texaco	765	482	0.26	49%
R13.2	182	Kingsport	750	482	0.15	43%
R13.3	286.5	Kingsport	735	482	0.34	48%
Catalyst B Runs						
R14.1	53	Texaco	765	482	0.26	44%
R14.2	170.5	Kingsport	750	482	0.15	39%
R14.3	138	Kingsport	535	482	0.36	42%
R14.4	172	Texaco	765	482	0.14	41%
R14.5	202	Texaco	765	482	0.25	45%
R14.9	5	Kingsport	765	482	0.046	40%

Table 2. Comparison of average gas holdup values and solids loading obtained using differential pressures, gamma densitometry and shutdown tests for catalyst A runs.

			Densitometry		Pressures		Shutdown
Run No.	Gas Type	U_G (m/s)	Gas Holdup	Catalyst Loading	Gas Holdup	Catalyst Loading	Gas Holdup
R13.1A	Texaco	0.26	50.5%	45.8%	45.4%	48.4%	
R13.1B	Texaco	0.26	54.7%	48.2%	47.0%	49.4%	
R13.2A	Kingsport	0.15	42.3%	41.7%	35.3%	43.0%	
R13.2B	Kingsport	0.15	43.1%	42.0%			35.2%
R13.3A	Kingsport	0.34	55.7%	48.5%	44.5%	47.7%	
R13.3B	Kingsport	0.34	55.8%	48.9%	44.4%	48.0%	

Table 3. Comparison of average gas holdup values and solids loading obtained using differential pressures, gamma densitometry and shutdown tests for catalyst B runs.

			Densitometry		Pressures		Shutdown
Run No.	Gas Type	U_G (m/s)	Gas Holdup	Catalyst Loading	Gas Holdup	Catalyst Loading	Gas Holdup
R14.4	Texaco	0.14	42.9%	42.2%	33.0%	41.4%	
R14.1A	Texaco	0.26	49.6%	45.4%	38.3%	43.6%	
R14.1B	Texaco	0.26	49.9%	45.3%	38.8%	43.6%	41.8%
R14.5	Texaco	0.25	50.8%	46.5%	39.7%	44.9%	
R14.9	Kingsport	0.046	25.8%	41.2%	13.4%	40.5%	
R14.2A	Kingsport	0.15	37.5%	39.4%	28.1%	38.9%	
R14.2B	Kingsport	0.15	38.1%	39.7%	28.5%	39.1%	
R14.3	Kingsport	0.36	50.4%	45.6%	36.1%	42.3%	39.2%

Table 4. Mean gas holdup data for runs with catalyst A.

Run No.	U_G (m/s)	Gas Type	C to N2 L/D = 5.4	N2 to D L/D = 11.1	D to N1 L/D = 17.8	N1 to E L/D = 24.5
R13.1	0.26	Texaco	44.7%	42.4%	44.9%	52.8%
R13.2	0.15	Kingsport	34.5%	31.6%	33.8%	41.3%
R13.3	0.34	Kingsport	43.7%	41.1%	43.0%	50.2%

Table 5. Mean gas holdup data for runs with catalyst B.

Run No.	U_G (m/s)	Gas Type	C to N2 L/D = 5.4	N2 to D L/D = 11.1	D to N1 L/D = 17.8	N1 to E L/D = 24.5
R14.4	0.14	Texaco	32.1%	29.0%	32.2%	38.7%
R14.1	0.26	Texaco	37.7%	34.7%	37.7%	44.2%
R14.5	0.25	Texaco	38.2%	35.5%	38.5%	46.4%
R14.9	0.046	Kingsport	16.3%	11.4%	12.5%	
R14.2	0.15	Kingsport	28.8%	24.7%	27.0%	32.8%
R14.3	0.36	Kingsport	36.0%	32.8%	34.4%	41.1%

Table 6. Standard deviations in gas holdup data for runs with catalyst A.

Run No.	U_G (m/s)	Gas Type	C to N2 L/D = 5.4	N2 to D L/D = 11.1	D to N1 L/D = 17.8	N1 to E L/D = 24.5
R13.1	0.26	Texaco	0.65%	0.59%	0.49%	1.06%
R13.2	0.15	Kingsport	0.57%	0.45%	0.32%	0.89%
R13.3	0.34	Kingsport	0.93%	0.88%	0.71%	1.53%

Table 7. Standard deviations in gas holdup data for runs with catalyst B.

Run No.	U_G (m/s)	Gas Type	C to N2 L/D = 5.4	N2 to D L/D = 11.1	D to N1 L/D = 17.8	N1 to E L/D = 24.5
R14.4	0.14	Texaco	0.46%	0.38%	0.35%	1.04%
R14.1	0.26	Texaco	0.75%	0.71%	0.64%	1.30%
R14.5	0.25	Texaco	0.77%	0.71%	0.65%	1.29%
R14.9	0.046	Kingsport	0.32%	0.23%	0.31%	0.48%
R14.2	0.15	Kingsport	0.51%	0.44%	0.39%	0.84%
R14.3	0.36	Kingsport	1.05%	1.04%	0.88%	1.85%

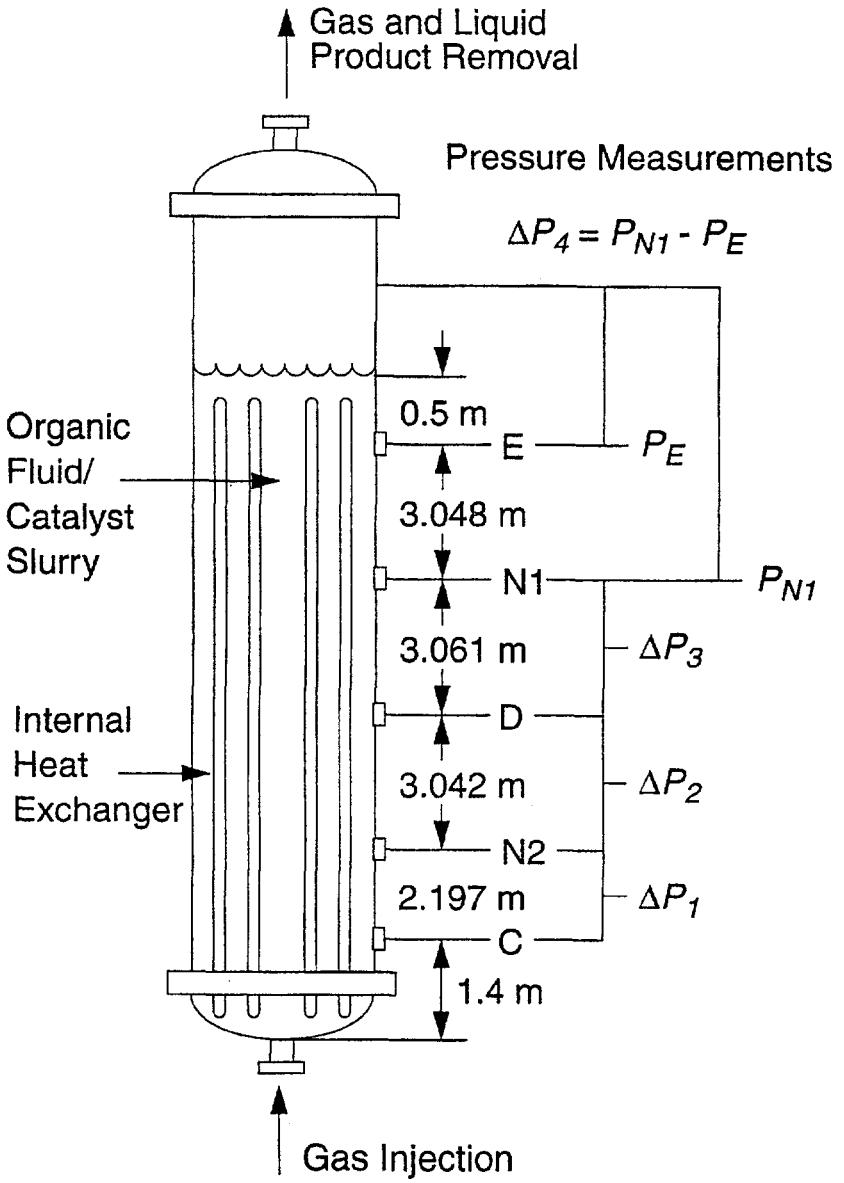

Figure 1. Schematic diagram of LaPorte Alternative Fuels Development Unit (AFDU); 18 in. (0.457 m) inside diameter, 50 ft. (15.24 m) normal liquid level during operation, 2000 psig (13.8 MPa) design pressure, 700 °F (371 °C) design temperature.

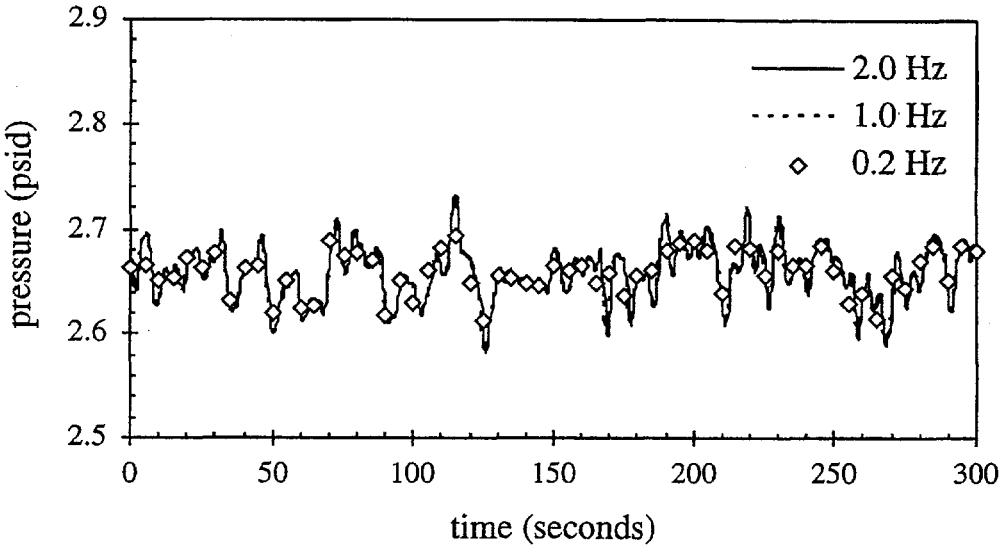

Figure 2. Time trace of differential pressure signal between nozzles N2 and D (L/D = 11.1) at different sampling rates for Run No. R13.1, $U_G = 0.26$ m/s, Texaco gas, $\omega_S = 49\%$, 765 psia (5.27 MPa), 482 °F (250 °C).

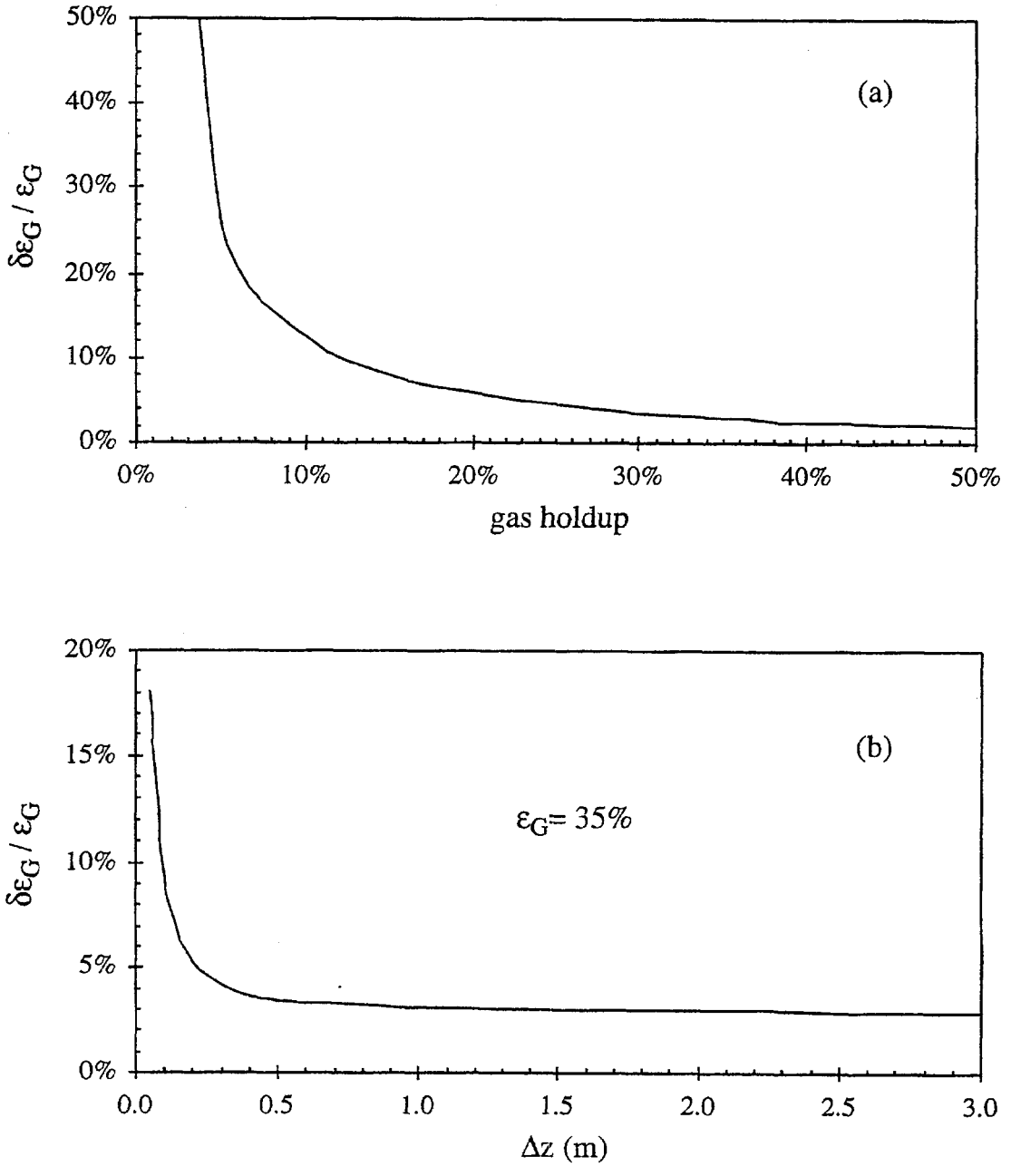

Figure 3. Relative uncertainty in gas holdup ($\delta\varepsilon_G/\varepsilon_G$) as function of (a) gas holdup and (b) distance between pressure taps under AFDU operating conditions, Texaco gas, and catalyst A.

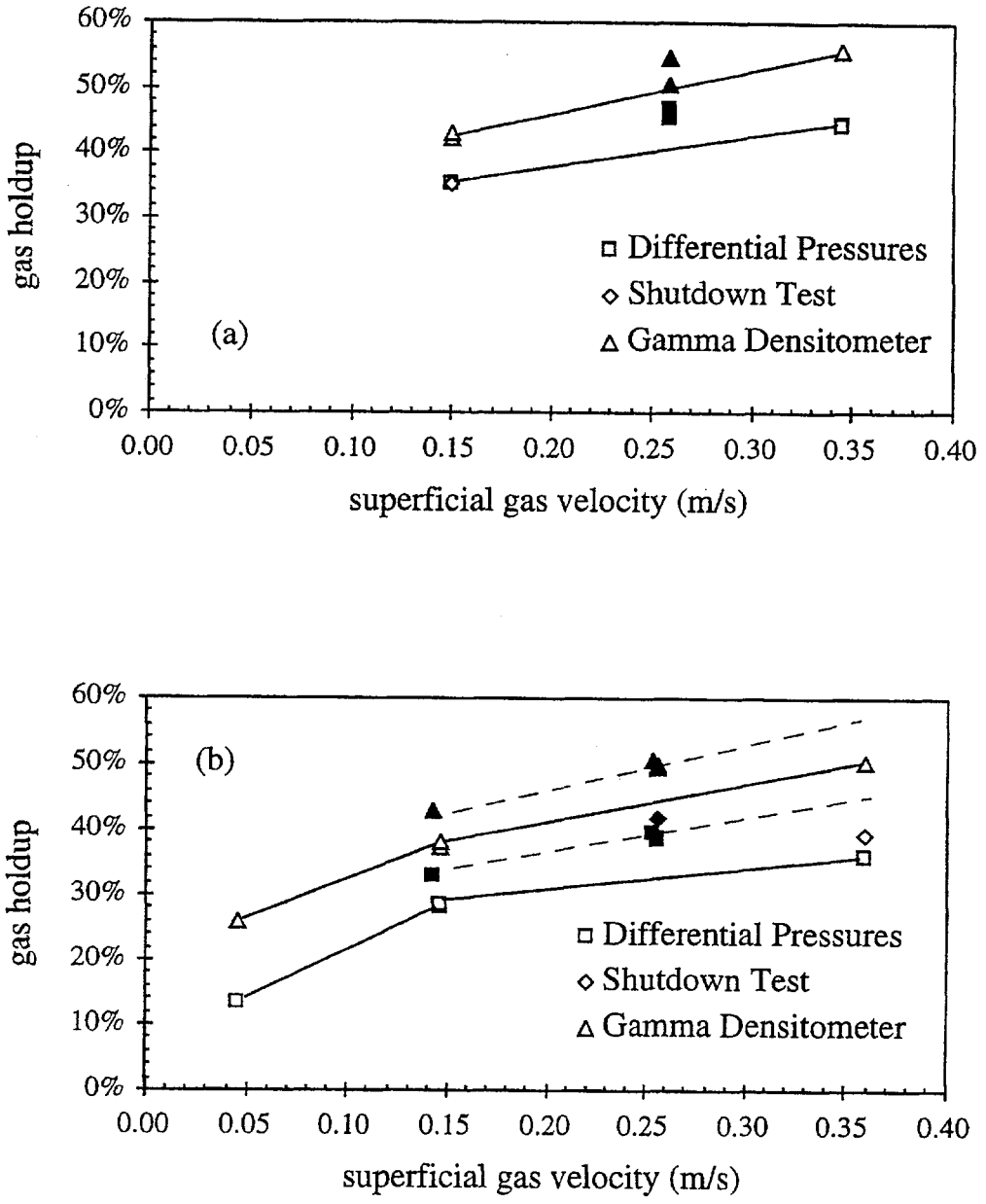

Figure 4. Comparison of gas holdups measured using differential pressures, gamma densitometer and shutdown test for (a) catalyst A runs (R13) and (b) catalyst B runs (R14); closed and open symbols denote Texaco and Kingsport gas, ω_S = 39%-49%, 535-765 psia (3.69-5.27 MPa), 482 °F (250 °C).

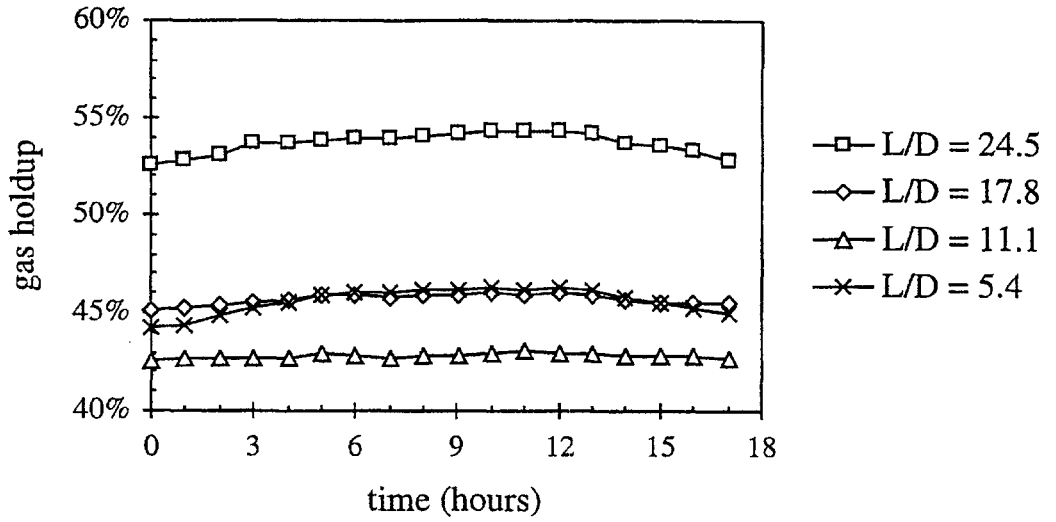

Figure 5. Gas holdups averaged over one-hour periods for catalyst A run number R13.1; U_G = 0.26 m/s, Texaco gas, ω_S = 49%, 765 psia (5.27 MPa), 482 °F (250 °C).

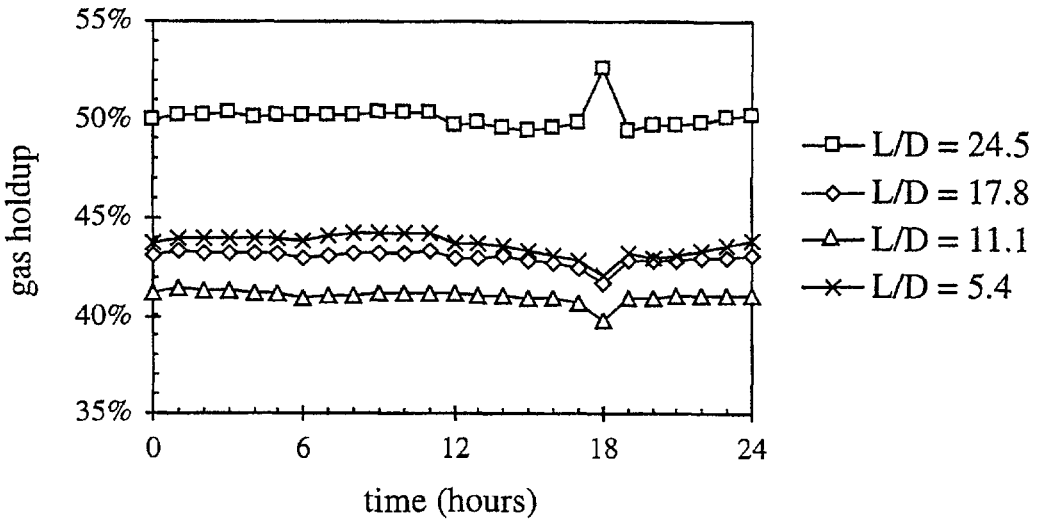

Figure 6. Gas holdups averaged over one-hour periods for catalyst A run number R13.3; U_G = 0.34 m/s, Kingsport gas, ω_S = 48%, 735 psia (5.07 MPa), 482 °F (250 °C).

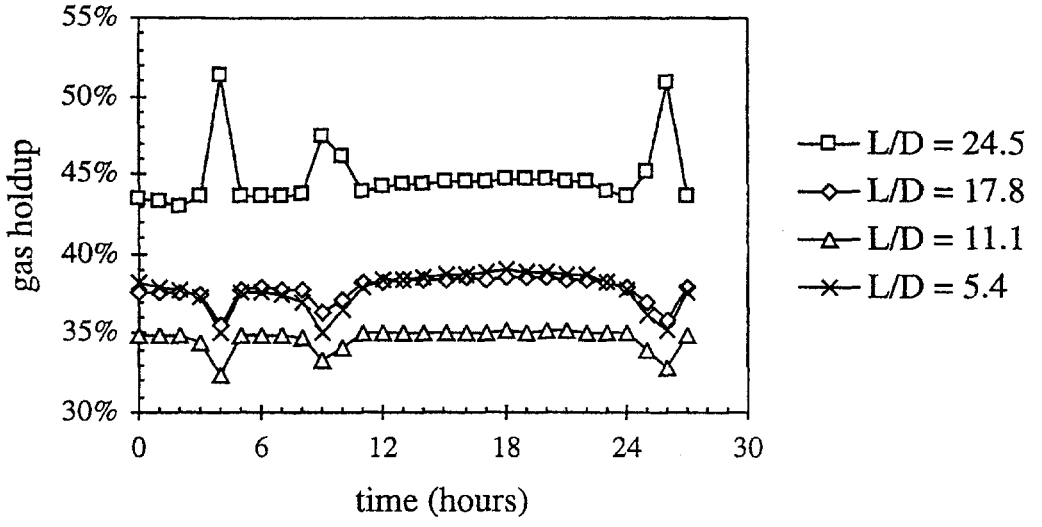

Figure 7. Gas holdups averaged over one-hour periods for catalyst B run number R14.1; U_G = 0.26 m/s, Texaco gas, ω_S = 44%, 765 psia (5.27 MPa), 482 °F (250 °C).

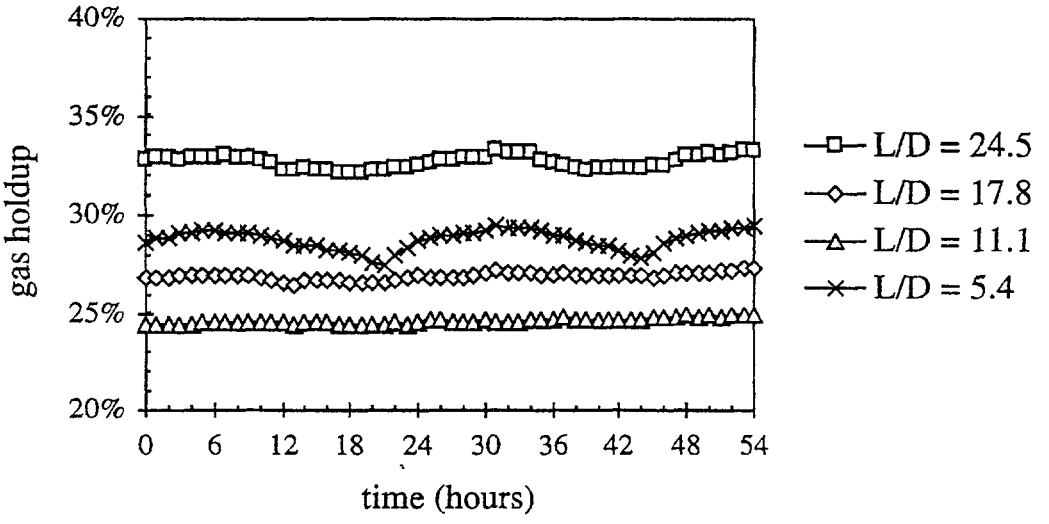

Figure 8. Gas holdups averaged over one-hour periods for catalyst B run number R14.2; U_G = 0.15 m/s, Kingsport gas, ω_S = 39%, 750 psia (5.17 MPa), 482 °F (250 °C).

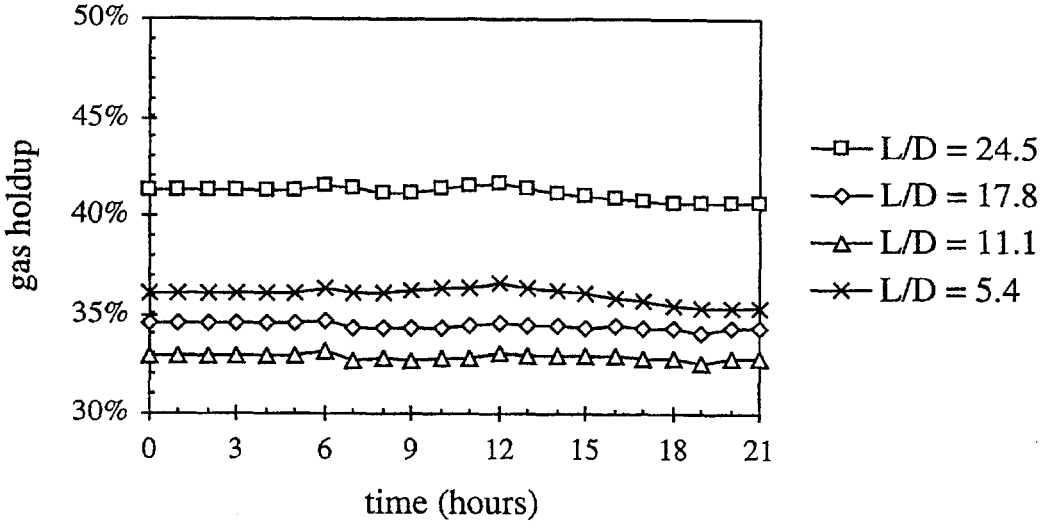

Figure 9. Gas holdups averaged over one-hour periods for catalyst B run number R14.3; U_G = 0.36 m/s, Kingsport gas, ω_S = 42%, 535 psia (3.69 MPa), 482 °F (250 °C).

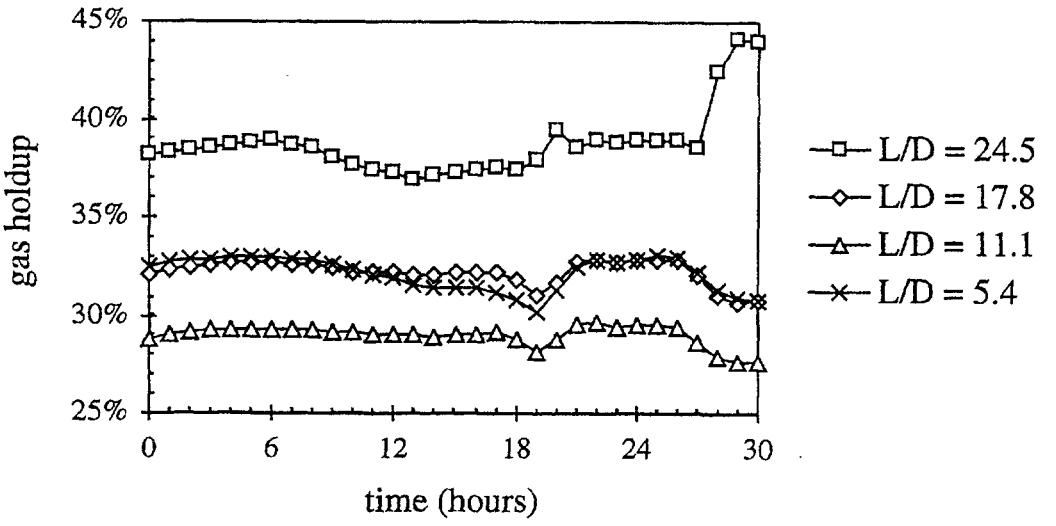

Figure 10. Gas holdups averaged over one-hour periods for catalyst B run number R14.4; U_G = 0.14 m/s, Texaco gas, ω_S = 41%, 765 psia (5.27 MPa), 482 °F (250 °C).

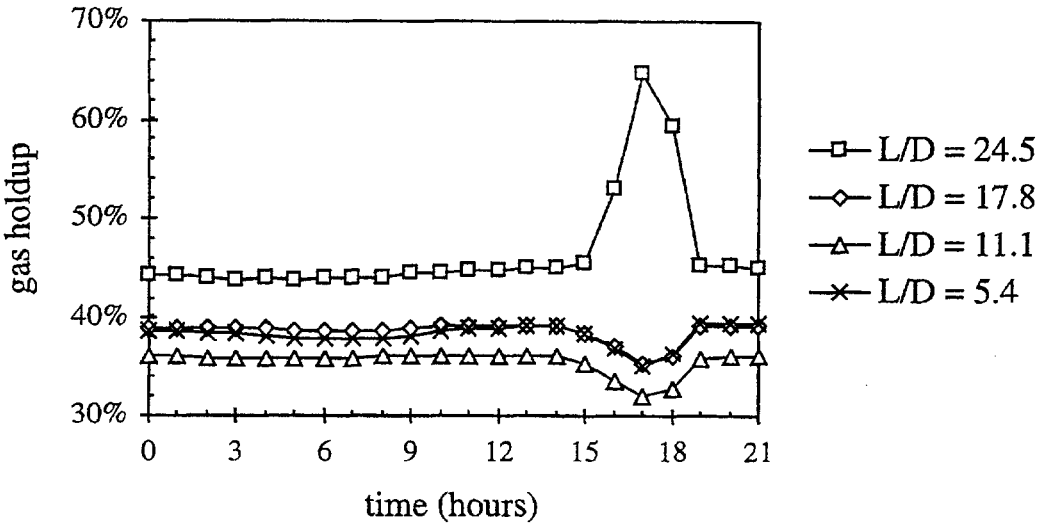

Figure 11. Gas holdups averaged over one-hour periods for catalyst B run number R14.5; U_G = 0.25 m/s, Texaco gas, ω_S = 45%, 765 psia (5.27 MPa), 482 °F (250 °C).

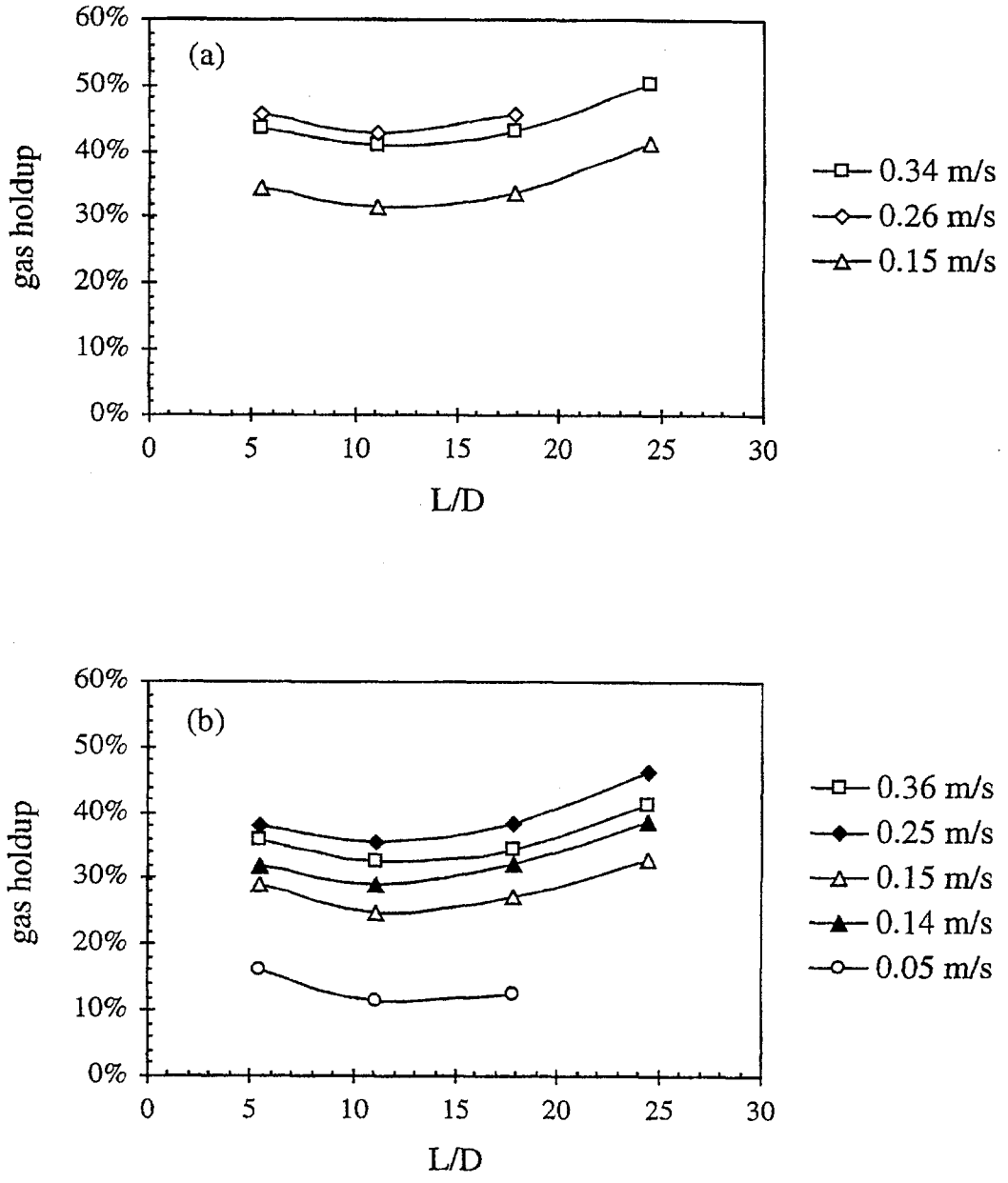

Figure 12. Gas holdup versus axial distance from sparger and superficial gas velocity in the AFDU for (a) catalyst A and (b) catalyst B; closed and open symbols denote Texaco and Kingsport gas, ω_S = 39-44%, 535-765 psia (3.69-5.27 MPa), 482 °F (250 °C).

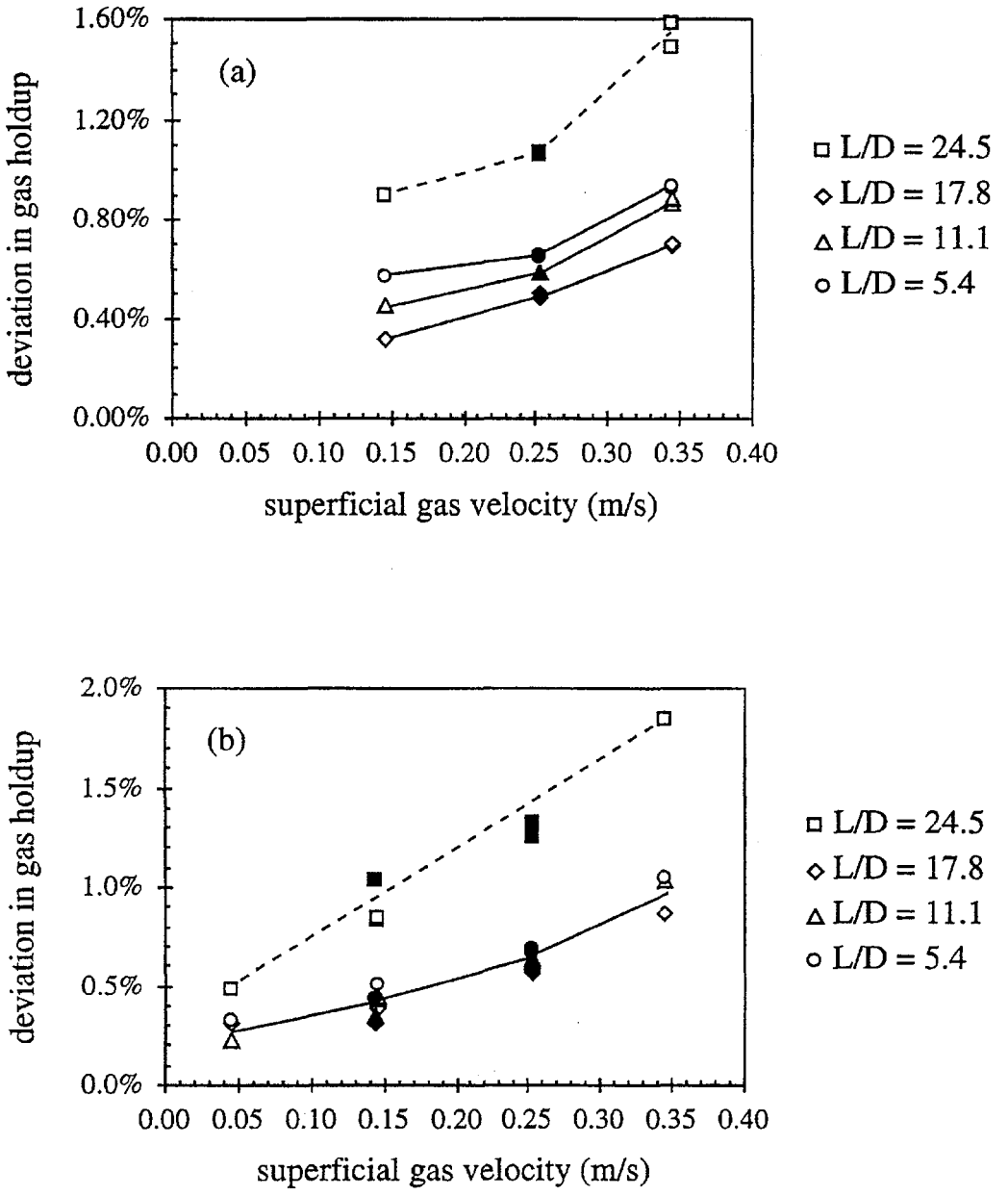

Figure 13. Standard deviation of gas holdup versus superficial gas velocity and axial distance from sparger in the AFDU for (a) catalyst A and (b) catalyst B; closed and open symbols denote Texaco and Kingsport gas, ω_S = 39-44%, 535-765 psia (3.69-5.27 MPa), 482 °F (250 °C).

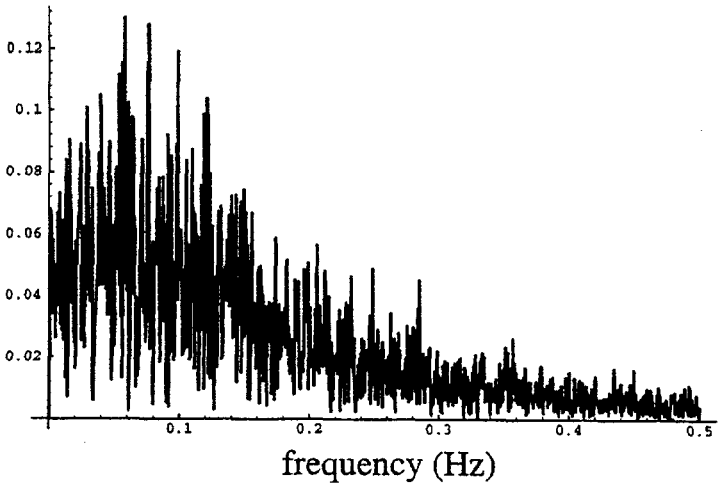

Figure 14. Frequency spectrum of differential pressure for catalyst B run number R14.3; $U_G = 0.36$ m/s, Kingsport gas; $\omega_S = 42\%$, 535 psia (3.69 MPa), 482 °F (250 °C).

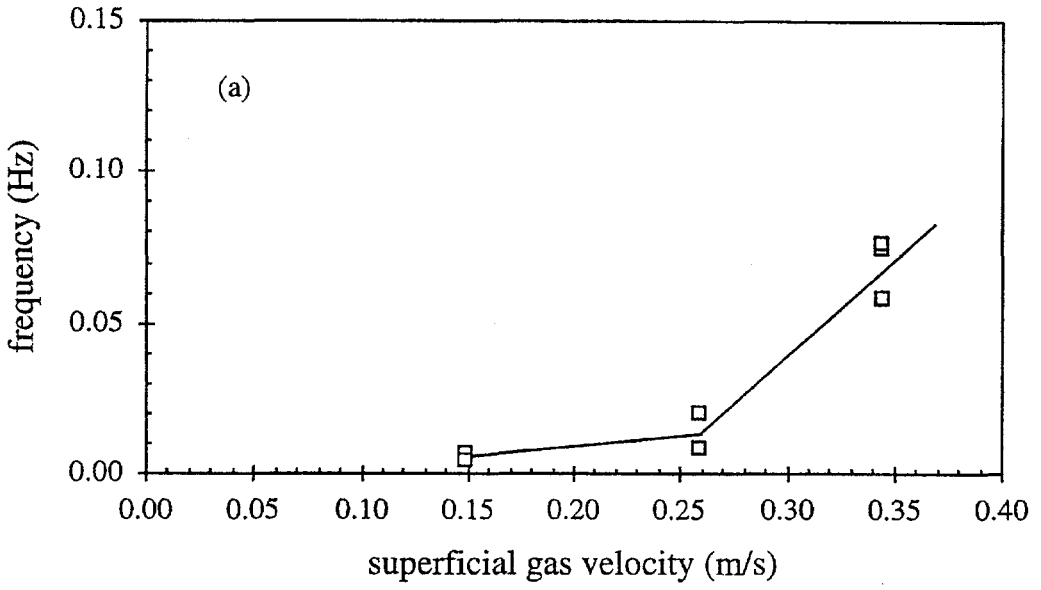

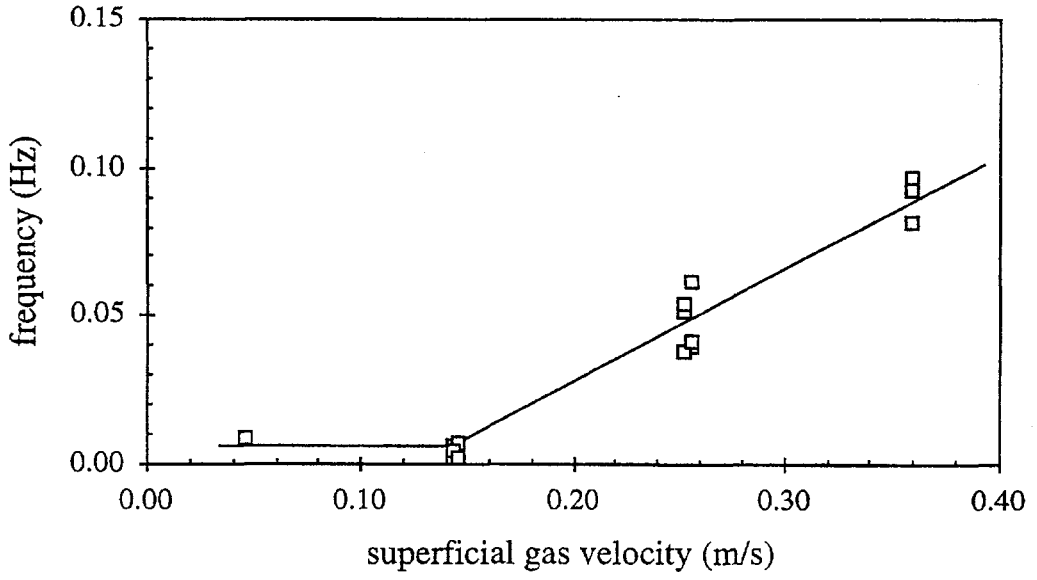

Figure 15. Dominant frequency component from Fourier analysis of differential pressures versus superficial gas velocity in the AFDU for (a) catalyst A and (b) catalyst B; ω_S = 39-44%, 535-765 psia (3.69-5.27 MPa), 482 °F (250 °C).

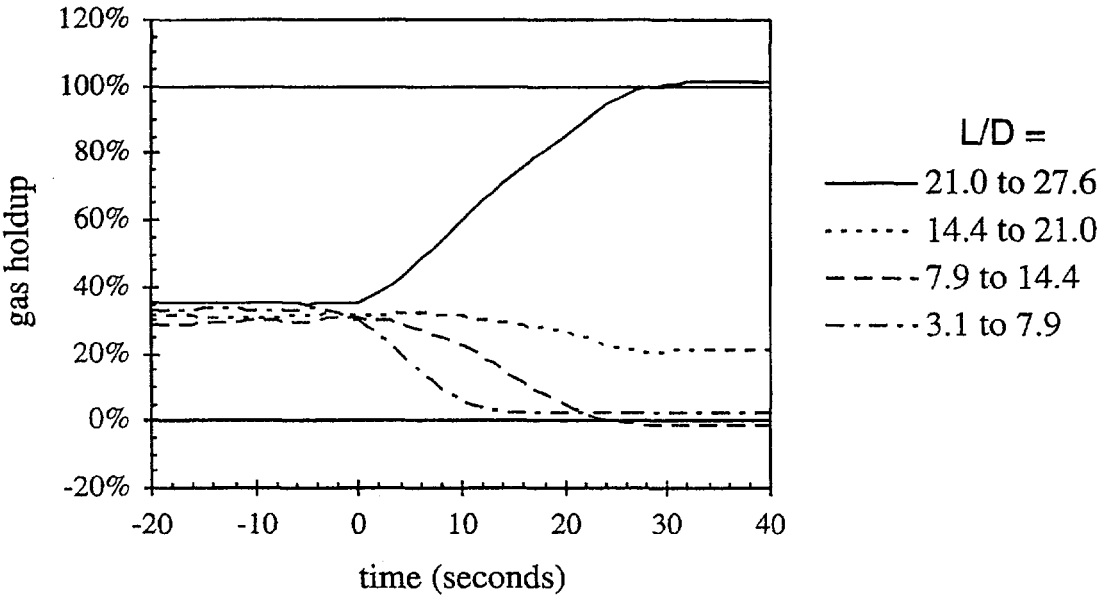

Figure 16. Dynamic Gas Disengagement curves from differential pressure measurements in AFDU for Run No. R13.2; $U_G = 0.15$ m/s, Kingsport gas, $\omega_S = 43\%$, catalyst A, 750 psia (5.17 MPa) and 482 °F (250 °C).

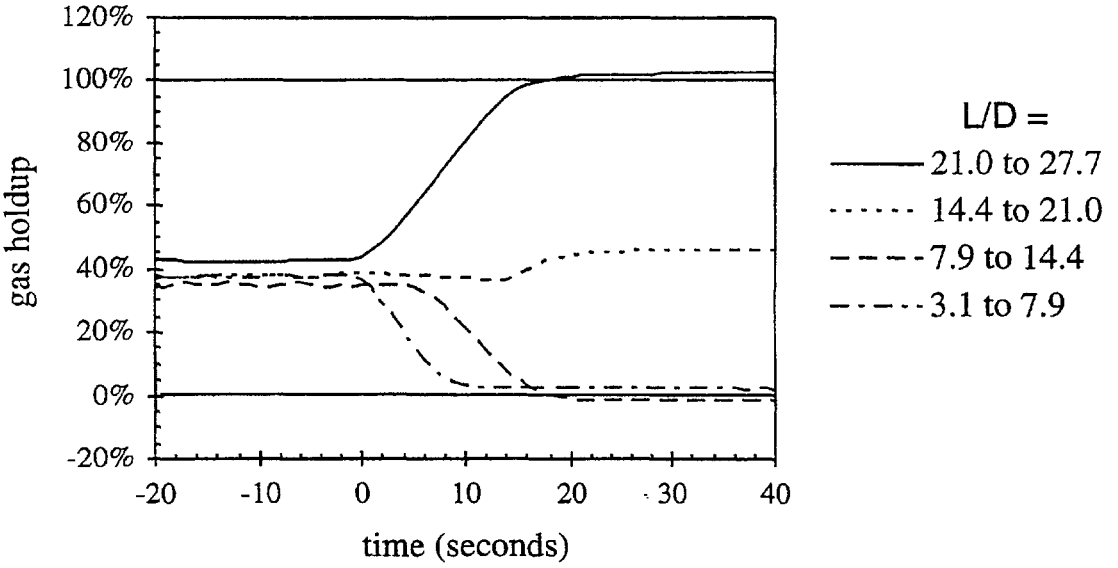

Figure 17. Dynamic Gas Disengagement curves from differential pressure measurements in AFDU for Run No. R14.1; $U_G = 0.25$ m/s, Texaco gas, $\omega_S = 43\%$, catalyst B, 765 psia (5.27 MPa) and 482 °F (250 °C).

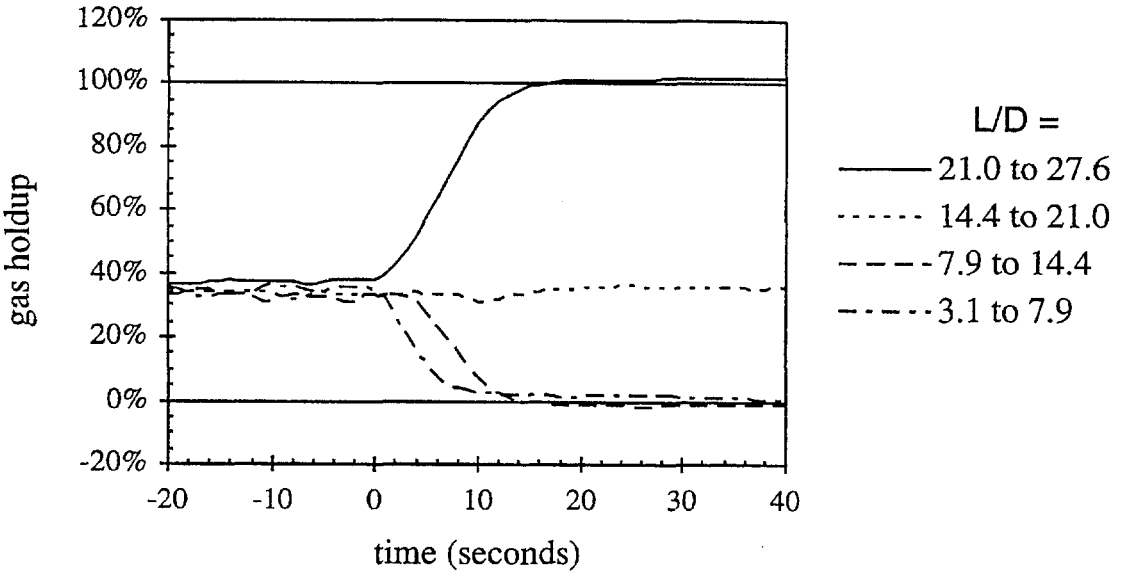

Figure 18. Dynamic Gas Disengagement curves from differential pressure measurements in AFDU for Run No. R14.3; $U_G = 0.36$ m/s, Kingsport gas, $\omega_S = 43\%$, 535 psia (3.69 MPa) and 482 °F (250 °C).

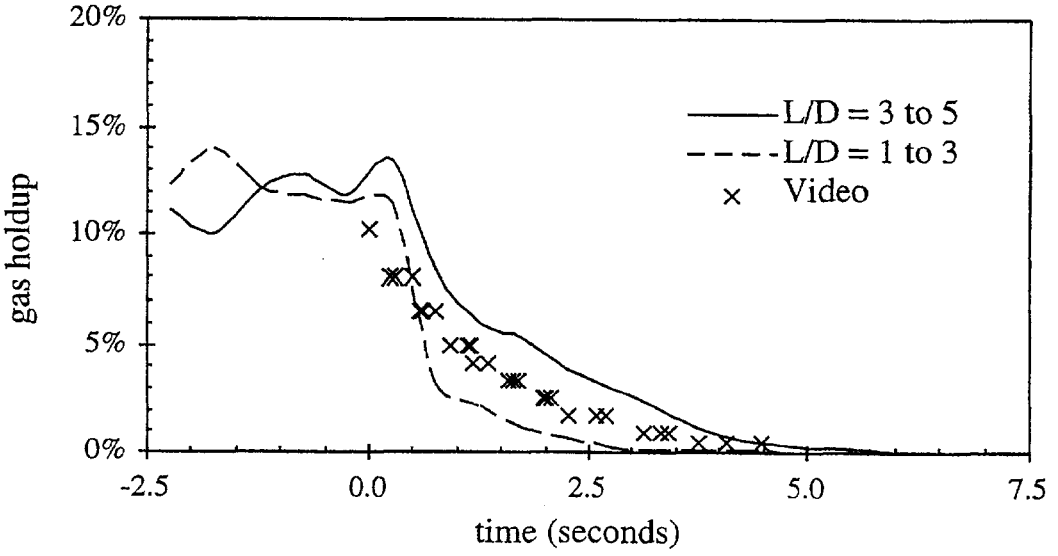

Figure 19. Dynamic Gas Disengagement curves from differential pressure measurements and high-speed video in 0.19 m Lexan column with air, water and 80 micron glass beads at atmospheric pressure and temperature; $U_G = 0.088$ m/s, $\omega_S = 40\%$.

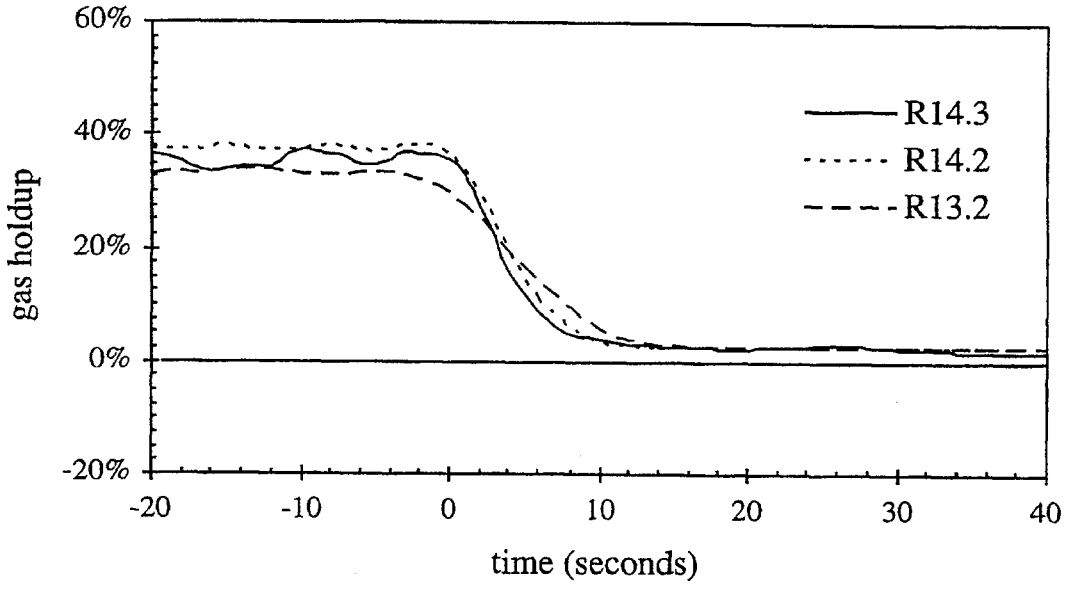

Figure 20. Dynamic Gas Disengagement curves in AFDU after run numbers R13.2, R14.1 and R14.3 at L/D between 3.1 and 7.9.

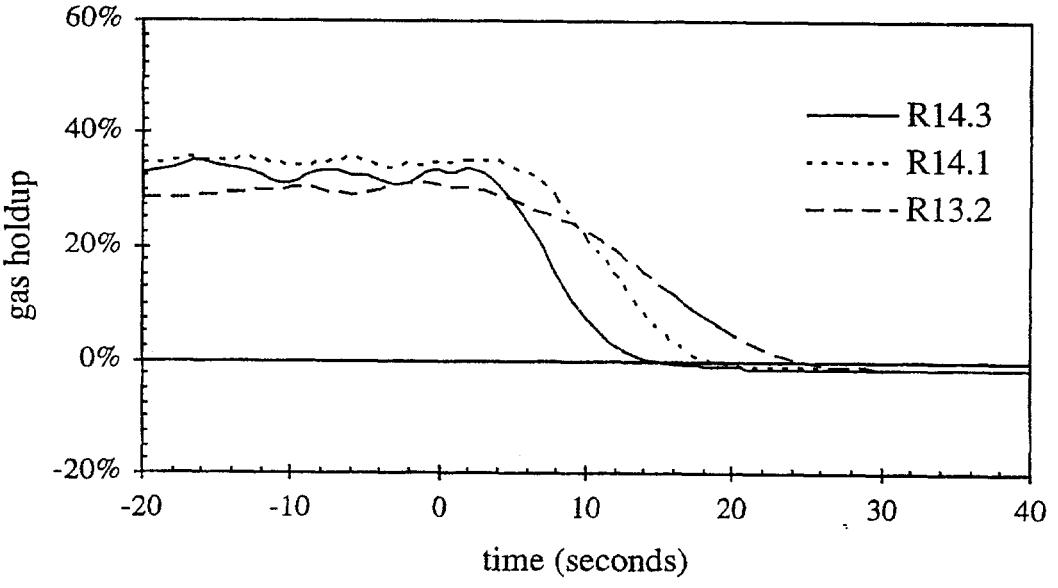

Figure 21. Dynamic Gas Disengagement curves in AFDU after run numbers R13.2, R14.1 and R14.3 at L/D between 7.9 and 14.4.

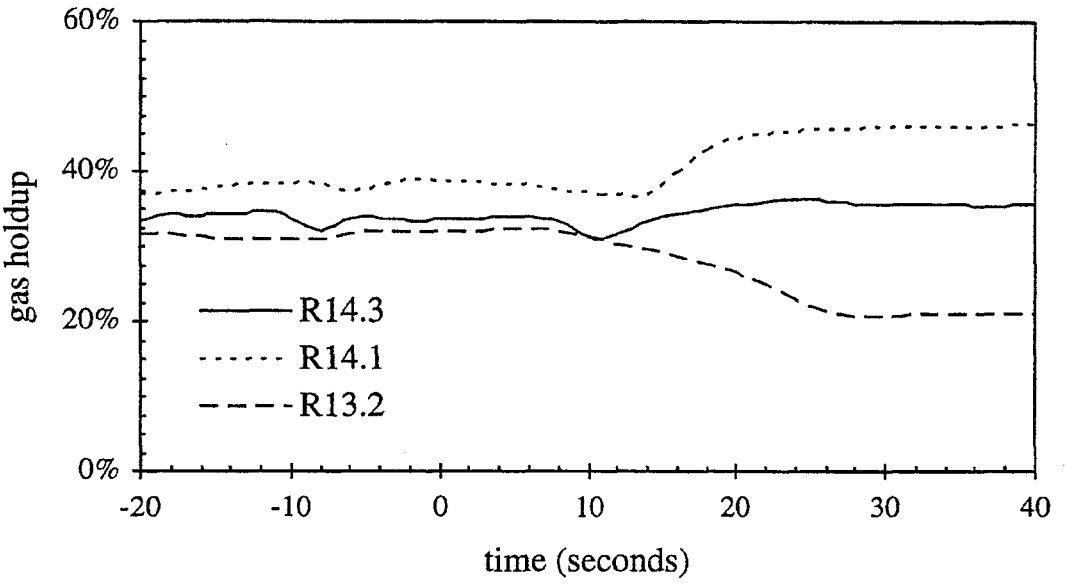

Figure 22. Dynamic Gas Disengagement curves in AFDU after run numbers R13.2, R14.1 and R14.3 at L/D between 14.4 and 21.0.

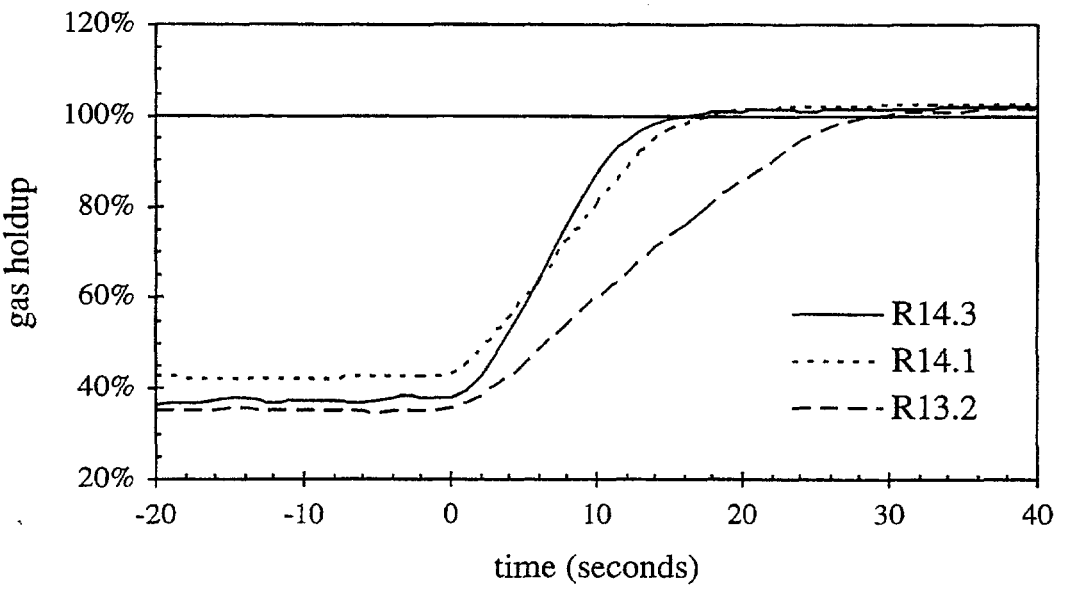

Figure 23. Dynamic Gas Disengagement curves in AFDU after run numbers R13.2, R14.1 and R14.3 at L/D between 21.0 and 27.6.

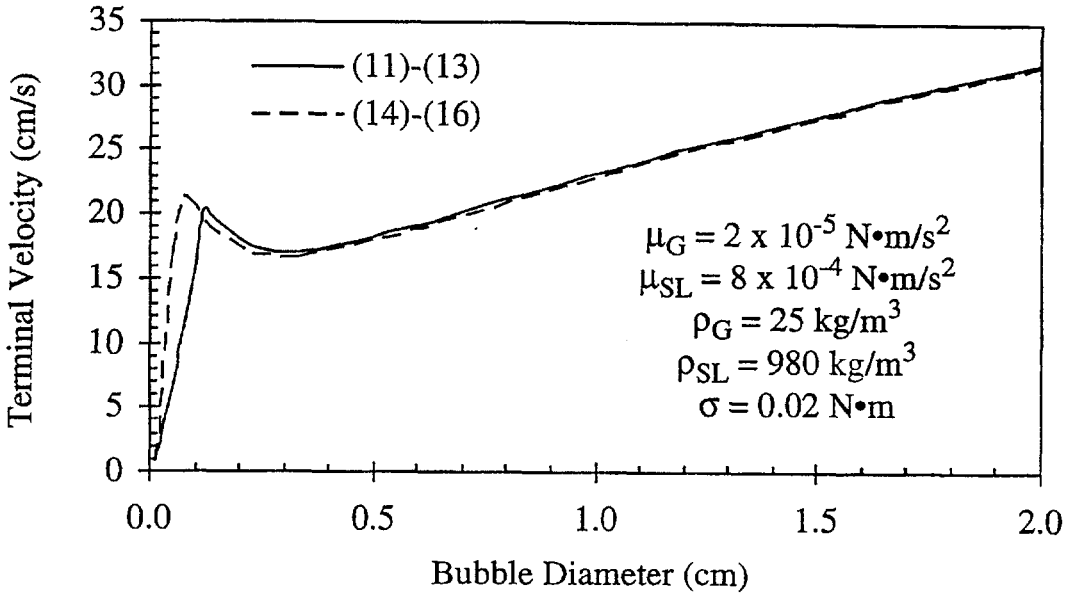

Figure 24. Comparison of terminal bubble velocity versus bubble diameter using (11)-(13) (Stokes' Law; Peebles and Garber, 1953; Clift et al., 1978) and (14)-(16) (a correlation by Jamialahmadi, 1994).

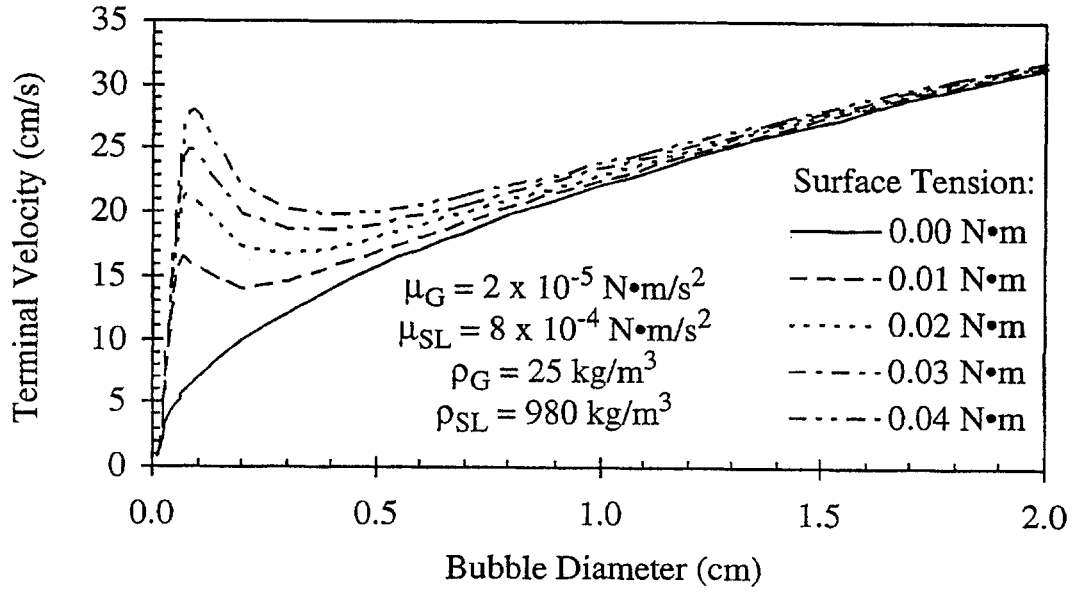

Figure 25. Terminal bubble velocity versus bubble diameter and surface tension using correlation by Jamialahmadi (1994).

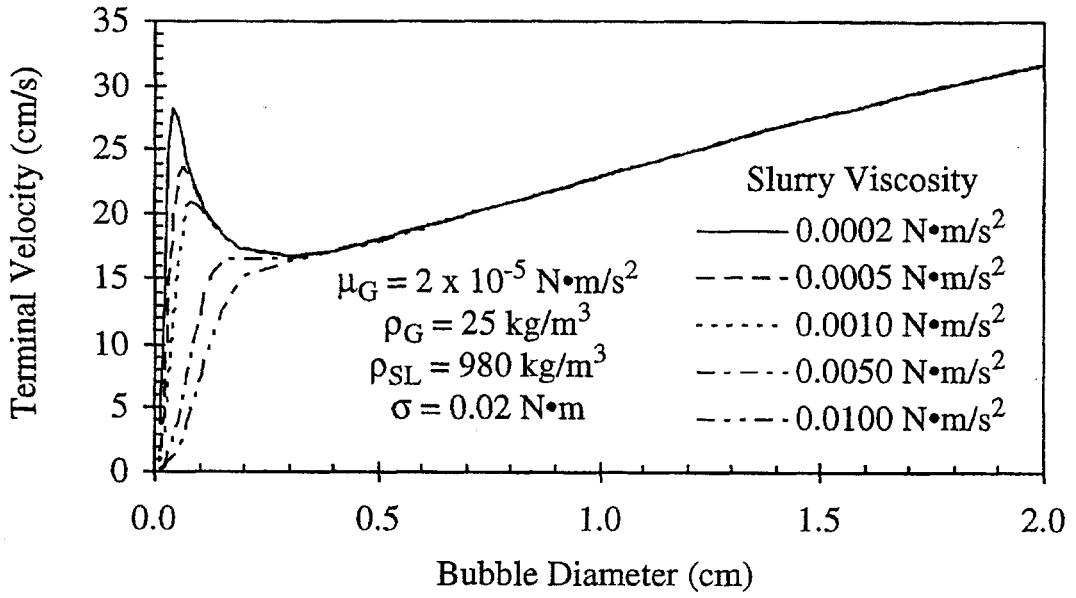

Figure 26. Terminal bubble velocity versus bubble diameter and liquid viscosity using correlation by Jamialahmadi (1994).

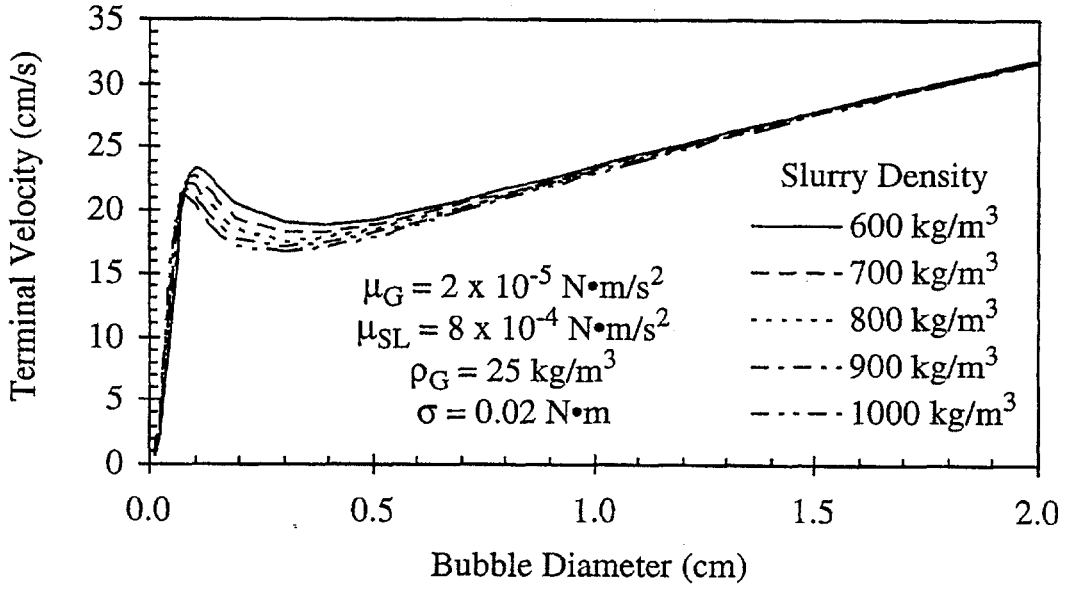

Figure 27. Terminal bubble velocity versus bubble diameter and liquid density using correlation by Jamialahmadi (1994).

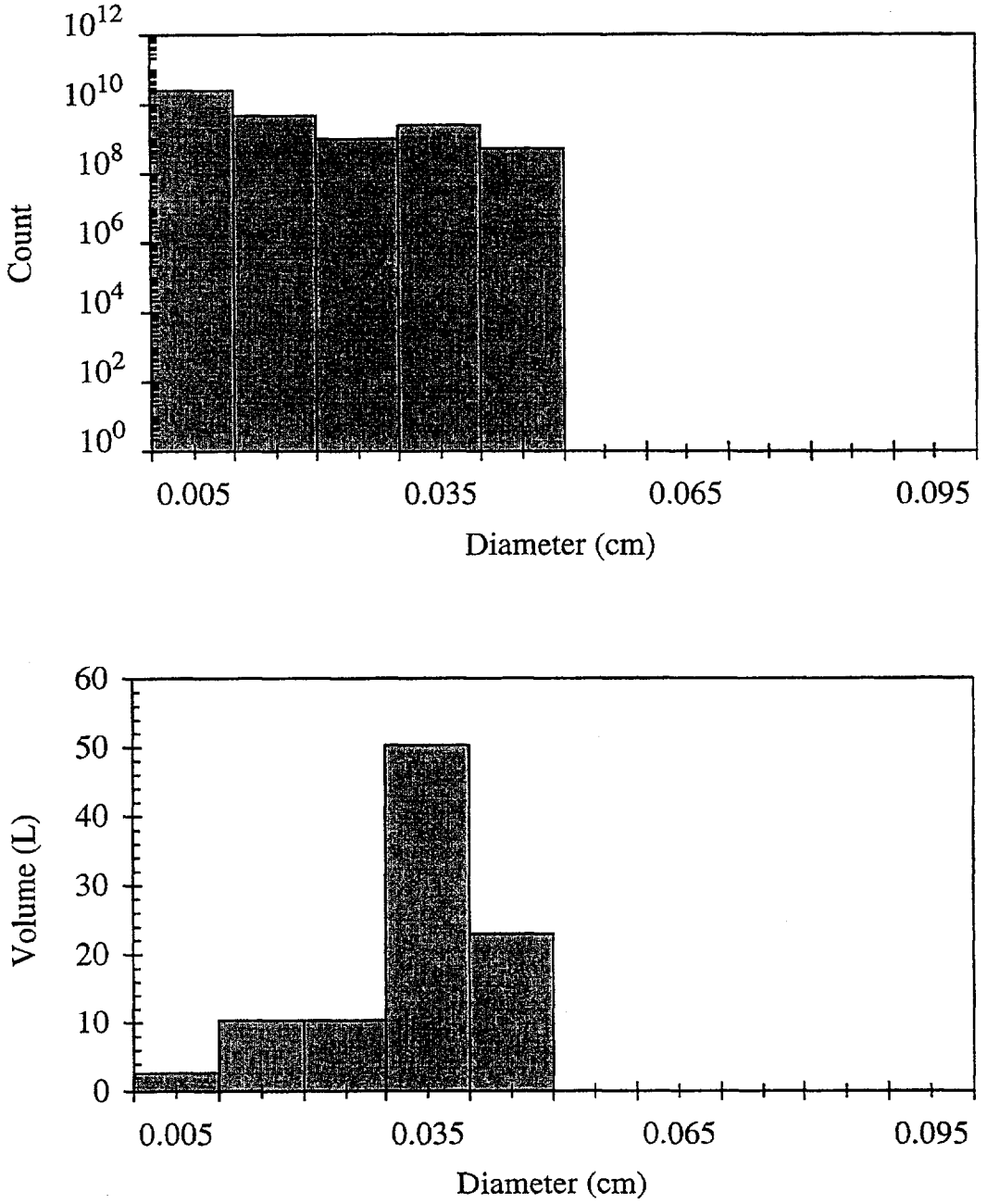

Figure 28. Number density and bubble volume histograms from DGD analysis and differential pressure measurements in AFDU for Run No. R13.2; $U_G = 0.15$ m/s, Kingsport gas, $\omega_S = 43\%$, catalyst A, 750 psia (5.17 MPa) and 482 °F (250 °C).

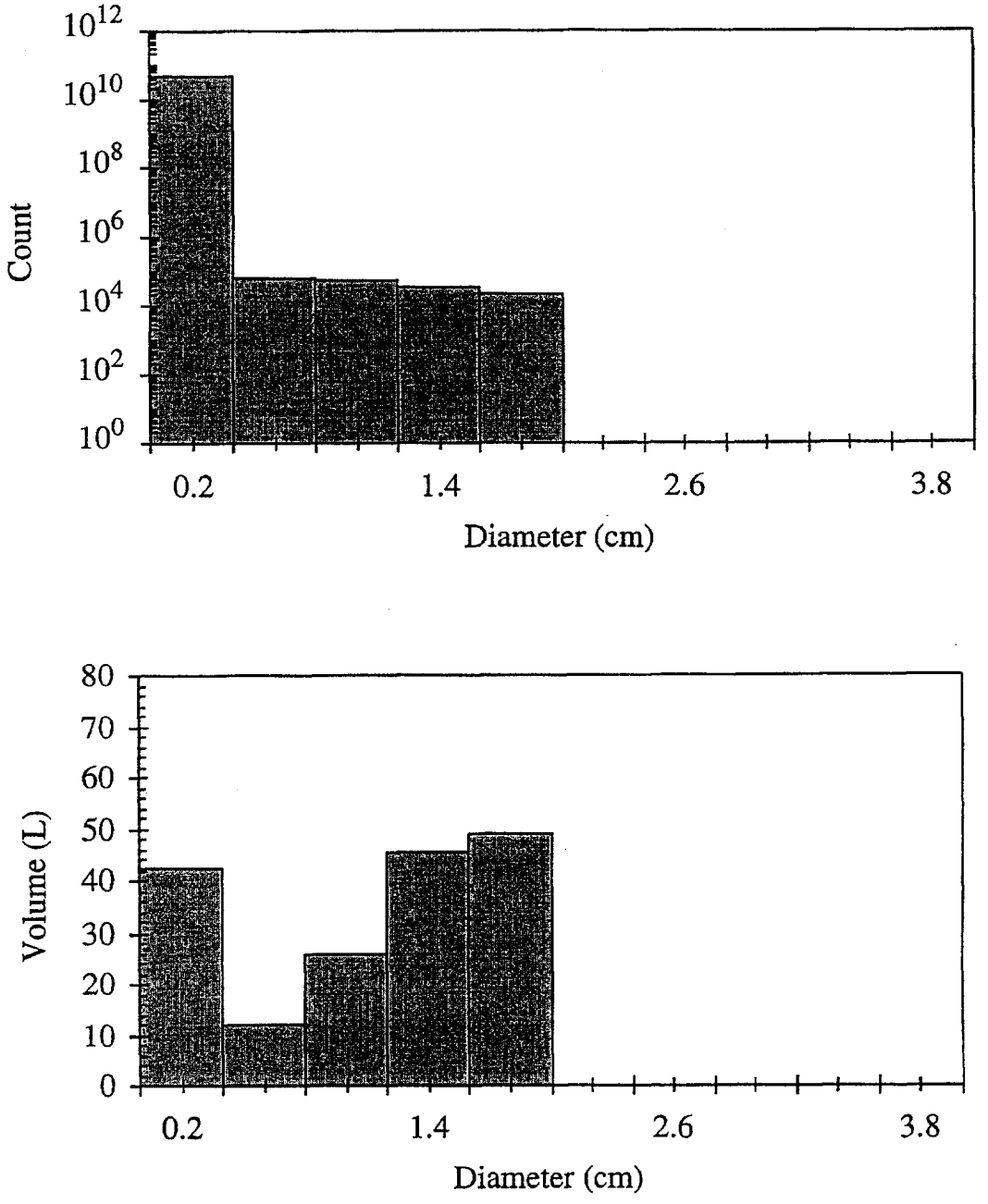

Figure 29. Number density and bubble volume histograms from DGD analysis and differential pressure measurements in AFDU for Run No. R14.1; $U_G = 0.25$ m/s, Texaco gas, $\omega_S = 43\%$, catalyst B, 750 psia (5.17 MPa) and 482 °F (250 °C).

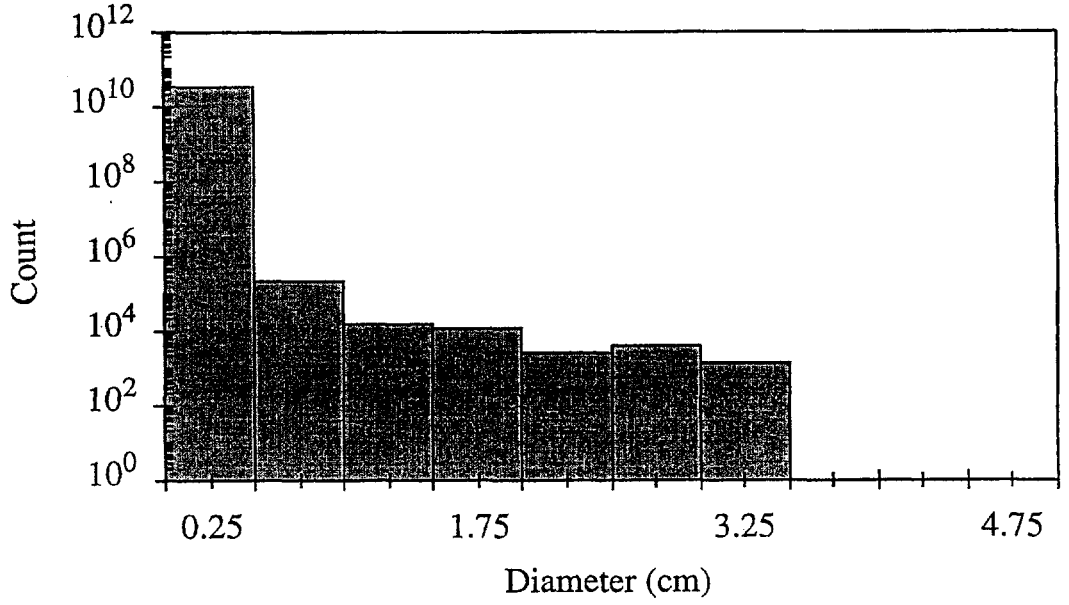

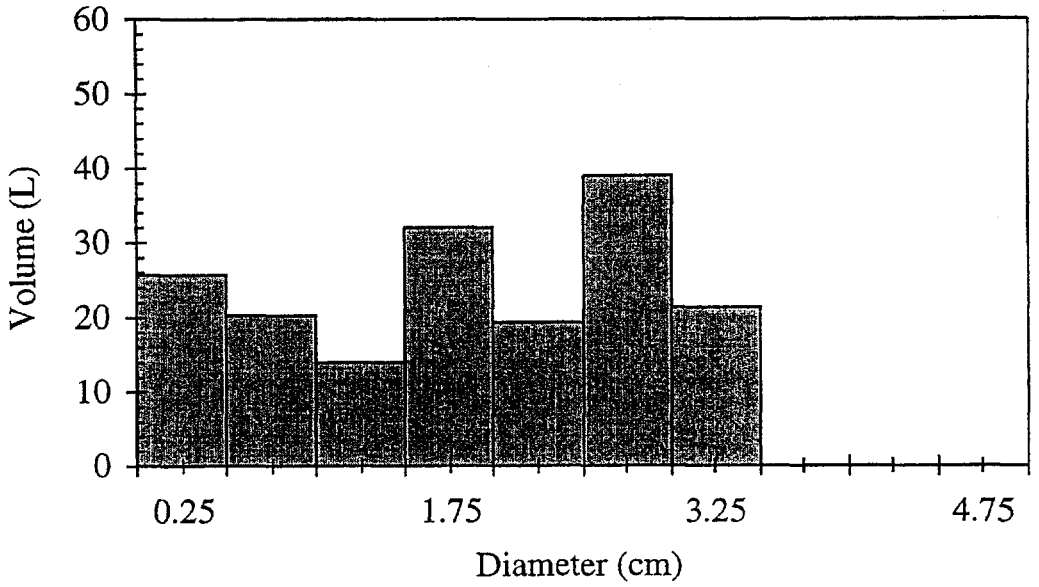

Figure 30. Number density and bubble volume histograms from DGD analysis and differential pressure measurements in AFDU for Run No. R14.3; $U_G = 0.36$ m/s, Kingsport gas, $\omega_S = 43\%$, catalyst B, 535 psia (3.69 MPa) and 482 °F (250 °C).